Contact metamorphism associated to the Penamacor–Monsanto granitic intrusion (Central Portugal): geochemical, isotopic and mineralogical features

Isabel Ribeiro da Costa, Isabel Margarida H. R. Antunes, Cyntia Mourão, Clemente Recio, Fernanda Guimarães, João Farinha Ramos [illegible]

Journal of Iberian Geology
Including Latin America and the Mediterranean

ISSN 1698-6180

J Iber Geol
DOI 10.1007/s41513-018-0050-x

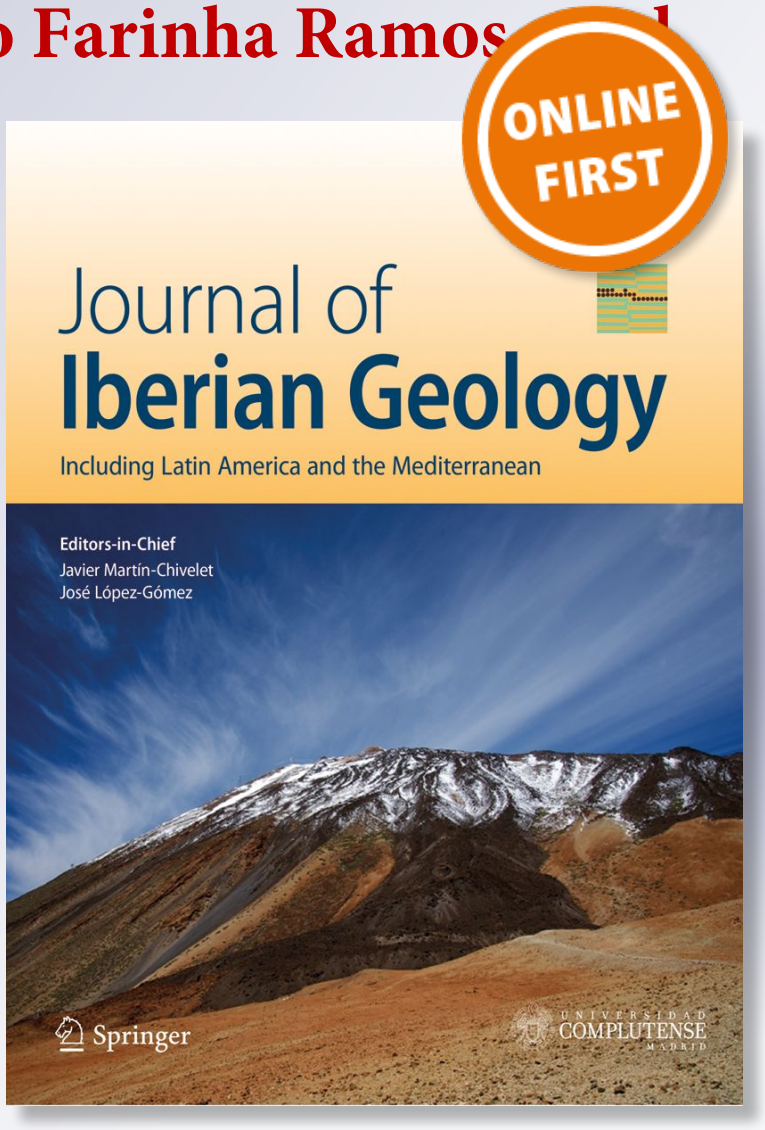

Springer

Journal of Iberian Geology
https://doi.org/10.1007/s41513-018-0050-x

RESEARCH PAPER

Contact metamorphism associated to the Penamacor–Monsanto granitic intrusion (Central Portugal): geochemical, isotopic and mineralogical features

Isabel Ribeiro da Costa[1] · Isabel Margarida H. R. Antunes[2] · Cyntia Mourão[1,3] · Clemente Recio[4] · Fernanda Guimarães[5] · João Farinha Ramos[3] · Fernando J. A. S. Barriga[1,3]

Received: 14 August 2017 / Accepted: 27 January 2018

Abstract

Contact metamorphism related to Variscan and late-Variscan granitic plutons in the Iberian Peninsula is superimposed on medium-grade regional metamorphism, making it often difficult to evaluate per se the thermal effects due to those intrusions and explaining the paucity of scientific literature on the subject. An exhaustive set of geochemical, isotopic and mineralogical data on the contact-zone metasediments hosting the Penamacor–Monsanto granite (Central Iberian Zone, Portugal) provides a significant contribution to the characterization of low- to intermediate-grade contact metamorphism in geological contexts formerly affected by regional metamorphism. The metasediments hosting the Penamacor–Monsanto pluton belong to the extensive detrital sequence of the ante-Ordovician Schist-Greywacke Complex. Bulk geochemistry, oxygen isotope data and crystal-chemistry of key minerals from those contact-zone and neighbouring metasediments have made it possible to infer metamorphic conditions on the contact zone of this granitic intrusion, and to distinguish them from late boron-metasomatism at the exocontact. Mineral parageneses (muscovite + biotite + chlorite ± quartz ± plagioclase ± cordierite, in spotted-schists; biotite + chlorite ± quartz ± plagioclase (± cordierite), in hornfelses) and the composition of these coexisting mineral phases indicate that most of the contact rocks reached the *biotite zone* (or even the *cordierite zone*, in some cases), equivalent to upper greenschist – lower amphibolite metamorphic grade. The relatively narrow range of O-isotope temperatures estimated for the crystallization of the marginal granites (550–625 °C) explains the absence of significant effects of thermal flow anisotropy on the contact-zone rocks. Besides, textural, paragenetic, mineralogical, isotopic and geochemical *nuances* observed in hornfelses and spotted-schists seem mainly related to the local host-rock heterogeneities, rather than to thermal effects. The relatively low temperatures estimated for granitoid emplacement and their restricted isotopic and mineralogical impacts on the metasedimentary host-rocks account for the narrow metamorphic aureole associated with the Penamacor–Monsanto pluton, and suggest this massif may correspond to the outcropping tip of a larger granitic intrusion at depth.

Keywords Penamacor–Monsanto pluton · Thermal metamorphism · Spotted-schists · Hornfelses · Metasediments

Resumen

Las intrusions graníticas Varíscicas y tardivaríscicas de la Península Ibérica dieron lugar a un metamorfismo de contacto que afecta a un encajante previamente sometido a un metamorfismo regional de grado medio, lo que dificulta separar los efectos térmicos de aquellos regionales, y explica la escasez de estudios sobre el mismo. El estudio detallado de la zona de contacto entre el Granito de Penamacor-Monsanto (Zona Centro-Ibérica; Portugal) y su encajante metasedimentario mediante técnicas geoquímicas, mineralógicas e isotópicas supone una notable contribución al conocimiento y caracterización del metamorfismo de contacto de grados bajos a intermedios en contextos geológicos previamente afectados por metamorfismo regional. El encajante metasedimentario del Plutón de Penamacor-Monsanto es parte de la amplia secuencia

Electronic supplementary material The online version of this article (https://doi.org/10.1007/s41513-018-0050-x) contains supplementary material, which is available to authorized users.

Extended author information available on the last page of the article

Published online: 16 February 2018

detrítica ante-Ordovícia conocida como Complejo Esquisto-Grawackico. Datos geoquímicos de roca total y cristaloquímicos de los minerales más característicos, y relaciones isotópicas de oxígeno en la zona de contacto y metasedimentos aledaños permiten inferir las condiciones metamórficas en la zona de contacto de dicha intrusión, y diferenciarla de aquella afectada por metasomatismo tardío por B. La paragénesis mineral (muscovita + biotita + clorita ± cuarzo ± plagioclasa ± cordierita en los esquistos moteados; biotita + clorita ± cuarzo ± plagiclasa (± cordierita) en corneanas) y la composición de las fases minerales coexistentes indican que la mayoría de rocas del contacto alcanzaron la zona de la biotita (e incluso, en algunos casos, aquella de la cordierita), equivalente a la parte alta del grado metamórfico de los esquistos verdes, o a la parte baja de las anfibolitas. El rango relativamente pequeño de temperaturas de cristalización de los granitos marginales (550-625°C), calculado mediante isótopos de oxígeno, explica la carencia de anisotropías térmicas significativas en las rocas del contacto. Las sutiles diferencias texturales, paragenéticas, mineralógicas, isotópicas y geoquímicas en esquistos moteados y corneanas parecen relacionadas con heterogeneidades locales de los encajantes, y no con efectos térmicos diferenciados. Las temperaturas relativamente bajas estimadas durante la intrusión del granito de Penamacor-Monsanto, y el limitado efecto mineralógico e isotópico sobre el encajante metasedimentario, dan lugar a una aureola de contacto estrecha, y sugieren que este macizo puede corresponder al techo de una intrusión mayor en profundidad.

Palabras clave Plutón de Penamacor-Monsanto · metamorfismo térmico · esquistos moteados · corneanas · metasedimentos

1 Introduction

Contact metamorphism results from the considerable temperature gradients produced when ascending magma bodies intrude relatively cold host-rocks. As element mobility, diffusion and zoning in minerals greatly depend on thermal factors (e.g., Dowty 1980; Nabelek 1991), detailed crystal-chemistry of key minerals in contact metamorphic aureoles, as well as geochemical and isotopic studies, are essential to infer the thermal flow associated with igneous intrusions and any derived anisotropies affecting their respective metamorphic aureole (e.g., Miyashiro 1978, 1994; Pattison and Tracy 1991; Voll et al. 1991; Johnson 1992; Miller et al. 2004).

Metapelitic rocks in Northern and Central Portugal host a considerable number of late- or post-Variscan granite intrusions. The focus of the present study is placed on the geochemical, isotopic and mineralogical features of the metamorphic assemblages present in the contact aureole of the Penamacor–Monsanto (P–M) pluton, in an attempt to infer the metamorphic conditions on the contact zone and any thermal flow anisotropy resulting from the emplacement of different granite facies within this intrusion. Although the metapelitic host-rocks of the P–M granite pluton have been less affected by the Variscan regional imprint than most other granite settings in Northern Portugal, the contact aureole and the specific mineralogical changes due to this intrusion are relatively limited (Ribeiro da Costa et al. 2013), making it often difficult to compare and distinguish the thermal effects due to the intrusion of different marginal granite facies.

Notwithstanding these limitations, and the pervasive weathering affecting the host Schist-Greywacke Complex (SGC), the detailed bulk-rock geochemistry and oxygen isotope data and mineral chemistry of key minerals in the metamorphic aureole of the P–M granite intrusion discussed here constitute a good basis to characterize the thermal conditions during the emplacement of the P–M pluton and a relevant complement to the petrographic study of this contact aureole and its immediate vicinity (Ribeiro da Costa et al. 2013). Additionally, these results shed light on the importance of rock protolith in determining the specific mineral parageneses and in controlling the geochemical and isotopic features of low- to intermediate-grade metamorphic aureoles in metapelitic/metapsammitic contexts.

2 Geotectonic and metamorphic setting

The Central Iberian Zone (CIZ) corresponds to the axial domain of the Variscan orogenic belt in the Iberian Peninsula (e.g., Ribeiro et al. 1990) and shows evidence of the three main Variscan deformation and metamorphic events, D1–D3 (Conde et al. 2000; Ábalos et al. 2002).

Granitic magmatism of highly peraluminous character is abundant in the CIZ, where it is mainly late- to post-kinematic relative to the main Variscan deformation events (D1 and D2): several different granite suites frequently occur at the cores of D3 antiforms (e.g., Bea et al. 1987; Ferreira et al. 1987; Ribeiro et al. 1990; Ramírez and Grundvig 2000; Azevedo et al. 2005; Antunes et al. 2009; Neiva et al. 2009).

The P–M pluton is a late- to post-D3 intrusion (e.g., Ferreira et al. 1987; Dias et al. 1998; Gutiérrez-Alonso et al. 2011). This pluton is elongated in a NW–SE orientation, and belongs to the monzogranite suite (Oliveira et al. 1992), which is particularly widespread in the southern sector of the CIZ and consists mainly of allochthonous, zoned plutons emplaced in an epizonal domain (Castro et al. 2002; Villaseca et al. 2014). The P–M granites were characterized by Neiva and Campos (1992, 1993) and petrographic details of the marginal facies of the pluton were described

by Ribeiro da Costa et al. (2013). The P–M intrusion is primarily composed of tourmaline-bearing two-mica monzogranites typical of the CIZ monzongranite suite, and more rarely of granodiorites (Pesquera et al. 2013). Despite some heterogeneities in grain-size and degree of alteration, these granitic rocks constitute most of the P–M marginal facies, as muscovite-granites and aplites occur only occasionally along the pluton margins (Ribeiro da Costa et al. 2013, 2014).

The P–M monzogranites are typical S-type granitic rocks derived from anatexis of weathered pelitic metasediments (according to the criteria of White and Chappell 1988), as is common in this context and has been described previously (e.g., Ugidos 1990): the granites are strongly peraluminous (ASI = 1.17–1.46), with high Al_2O_3 (13.5–15.6%) and low CaO ($\leq$ 0.6%) contents (Ribeiro da Costa et al. 2014); the high fractionation indices of these granites (Rb/Ba > 1) are consistent with high melt fractions, as required for magma mobilization (London 1999). Oxygen isotope signatures for the P–M marginal granites ($\delta^{18}O_{V\text{-}SMOW}$ = 11.7 to 13.0 ‰; Ribeiro da Costa et al. 2014) fall within the typical $\delta^{18}O$ range for S-type granitic rocks derived from anatexis of Al-rich metasediments (10–14‰; Sheppard 1986), as is the case of Variscan belt granites (Pesquera et al. 2013). Such origin is also emphasised by the oxygen and boron isotope data obtained on the P–M granite tourmalines ($\delta^{18}O$ = 12.0–12.3‰ and $\delta^{11}B$ = − 11.31 to − 8.89‰; Ribeiro da Costa et al. 2014).

The thermometric methods of Blamart (1991) and Zheng (1993), based on experimental $\delta^{18}O$ fractionation factors between tourmaline and water, yield temperatures in the range of 550–625 °C (Fig. 1) and 500–575 °C, respectively, for the late crystallization stages of the P–M granites (Ribeiro da Costa et al. 2014).

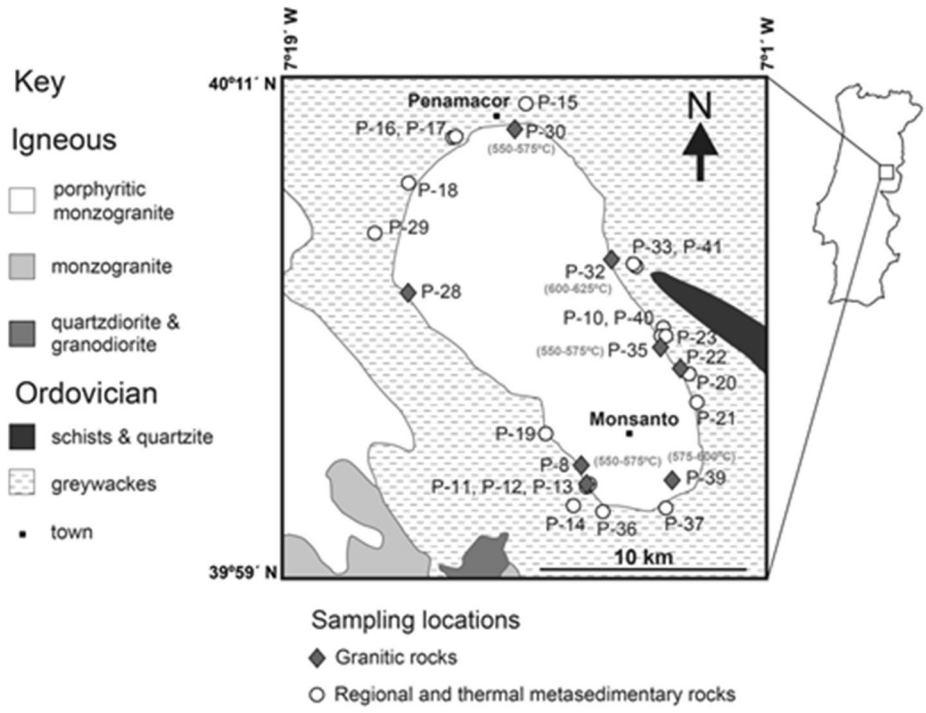

Samples used in this study:

Marginal granites

P-8, P-12, P-28, P-30, P-32, P-35, P-39 (data from Ribeiro da Costa et al. 2014)

Hornfelses

P-10, P-11, P-17, P-19, P-19B, P-21, P-22A, P-23,P-29, P-36A, P-37A, P-40, P-40B(2), P-41A

Spotted-schists

P-16, P-16A, P16B, P-18, P-18A, P-18B, P-18C, P-20, P-21A, P-22, P-36B, P-37B, P-40B(3)

Regional metasediments

P-13, P-14, P-15A, P-33A

Note: A, B or C has been added to sample references for samples collected within 4m from each other, in the same location, but exhibiting some macroscopic textural distinction.

Fig. 1 Simplified geological map of the Penamacor–Monsanto pluton in its regional context, showing sample locations (adapted from Ribeiro da Costa et al. 2014). Crystallization temperatures for Penamacor–Monsanto granites (according to the Blamart 1991 geothermometer; Ribeiro da Costa et al. 2014) are represented in light grey colour

Most of the Variscan granite plutons in the CIZ are surrounded by low-pressure, medium- to high-temperature metamorphic aureoles that overprint the polyphasic, low- to intermediate-pressure Variscan regional metamorphism (e.g., Oen 1970; Gama Pereira 1976; Reavy 1989; Ugidos 1990; Acciaioli et al. 2005). The P–M pluton is intrusive into low-grade metasedimentary rocks (typically chlorite zone) of the ante-Ordovician Schist-Greywacke Complex (SGC; Fig. 1), characterized by a thick and extensive *flysch*-type detrital sequence, mainly represented by fine- to very fine-grained phyllites, locally interrupted by metagreywackes with less marked or no foliation (Sousa 1985; Ribeiro et al. 1990; Ferreira Pinto and Matos 2000).

Accordingly, spotted-schists make up most of the narrow contact aureole produced by the P–M intrusion, while fine-grained granoblastic quartz-plagioclase hornfelses are restricted to a few locations within the innermost contact aureole (Ribeiro da Costa et al. 2013). As far as it can be mapped and individualized from the regional complex metamorphic history, this contact aureole ranges in width from 1000 to 2500 m (Neiva and Campos 1992) and also includes local tourmalinites (Ribeiro da Costa et al. 2013, 2014).

3 Sampling and analytical procedures

The present study has required extensive sampling of the P–M area (Fig. 1; Supplementary Data File: Sampling), namely: marginal granitic rocks from the pluton (two-mica granites and aplites); contact-zone rocks from the best exposed locations, least affected by weathering (hornfelses and spotted-schists); and regional metasedimentary rocks, collected near the contact zone, and used for comparison.

Whole-rock geochemical data for granitic rocks and contact zone rocks were determined at ACTLABS (Activation Laboratories, Ancaster, Ontario, Canada), by Fusion-ICP-MS (major and most trace-elements), INAA-Neutron Activation Analysis (rare-earth elements, REE), PGNAA-Prompt Gamma Neutron Activation Analysis (boron), Fusion-ISE Ion Selective Electrode Analysis (fluorine), and titration (ferrous iron). Accuracy was < 0.6% for SiO_2 and Al_2O_3, < 0.4% for FeO, Fe_2O_3, MgO, CaO and Na_2O, < 0.05% for K_2O, TiO_2 and P_2O_5, < 20 ppm for Ba, Cr, Ni, Cu, V and Zr, < 10 ppm for Sr and Rb, < 5 ppm for the REE, and < 1–2 ppm for the other trace elements.

Mineral compositions (Supplementary Data File: Mineral Chemistry) and X-ray elemental maps were obtained on a JEOL JXA-8500F electron microprobe (EMP), at LNEG (Laboratório Nacional de Energia e Geologia, S. Mamede de Infesta, Portugal). For analytical purposes, the microprobe was operated at 15 kV and 10 nA, with a mean electron beam diameter of 3–5 µm, and counting times of 20 s at analytical peaks and 10 s at the lower and upper backgrounds. Standards used were orthoclase (Si, Al, K, Ba), albite (Na), apatite (Ca), MgO (Mg), Fe_2O_3 (Fe), Mn-standard (Mn), TiO_2 (Ti), and fluorite (F). ZAF corrections were applied. Accuracy was ≤ 1% for the elements analysed.

Oxygen isotope data on the granites and regional rocks were determined at the Servicio General de Análisis de Isótopos Estables (University of Salamanca, Spain). Oxygen isotope ratios were determined by laser fluorination (Clayton and Mayeda 1963), employing a Synrad 25 W CO_2 laser (e.g., Sharp 1990) and ClF_3 as reagent (e.g., Borthwick and Harmon 1982). Isotope ratios were measured on a VG-Isotech SIRA-II dual-inlet mass spectrometer. International reference standards (NBS-28, NBS-30) were run to check accuracy and precision. Results are reported in the delta notation relative to the V-SMOW (Vienna Standard Mean Ocean Water) international standard, using a $\delta^{18}O$ value of 9.6‰ for NBS-28 [quartz] for the mass spectrometer calibration. Long-term reproducibility for repeated determination of $\delta^{18}O$ on reference samples was better than ± 0.2‰ (1σ).

4 Results

4.1 Contact aureole: whole-rock geochemistry and oxygen isotope data

Bulk-rock compositions of the contact rocks and neighbouring regional metasediments are presented in Table 1.

The P–M host-rocks conform to the geochemical criteria of Valladares et al. (1993), quite matching the Lower Series of the SGC (Upper Precambrian), and to the geochemical patterns of Lower Precambrian to Ordovician SGC metasediments (Beetsma 1995), as evidenced by the excellent correlations of K_2O, ($Fe_2O_3^T$ + MgO), TiO_2 and total REE with Al_2O_3 contents (Fig. 2a–d), and the rough correlations between SiO_2 and Rb/Zr ratios and the contact-rock alteration indices (AI = (MgO + K_2O)/(MgO + CaO + Na_2O + K_2O), Ishikawa et al. 1976) (Fig. 3a, b).

Concurring with the observed textural features, the SiO_2 and Al_2O_3 contents of the contact-zone rocks (Table 1) are a good indicator of their original precursors (Figs. 2 and 3a): hornfelses, with SiO_2 > 75 wt % and Al_2O_3 = 9–12 wt%, are obviously related to regional metapsammites and metagreywackes (e.g., samples P-15A and P-33A), whereas spotted-schists, exhibiting much lower SiO_2 contents (58–71 wt%) and Al_2O_3 > 14 wt%, closely resemble regional metapelites (e.g., samples P-13 and P-14), evidencing the dominance of phyllosilicates in their composition.

Oxidation in the P–M contact and regional rocks is quite variable along the metamorphic aureole and does not seem directly related to their alteration indices (Table 1; Fig. 3c),

Table 1 Bulk-rock geochemistry and oxygen isotope composition of the Penamacor–Monsanto contact zone metamorphic rocks and regional metasedimentary host-rocks (major components in wt%, trace-elements in ppm)

Sample	Regional Metasediments				Spotted-Schists										Hornfelses							
Reference	P-13	P-14	P-15A	P-33A	P-16	P-18	P-18A	P-18B	P-20	P-21A	P-36B	P-37B	P-37B(1)	P-40B(3)	P-19	P-19B	P-21	P-23	P-29	P-36A	P-40	P-40B(2)
SiO_2	69.7	60.8	80.1	77.6	66.5	63.2	60.6	64.1	60.7	70.9	58.8	69.3	70.1	69.1	75.6	83.1	80.4	75.7	79.7	78.6	81.1	79.7
TiO_2	0.83	0.86	0.46	0.51	0.84	1.06	0.98	0.75	1.03	0.68	0.99	0.77	0.82	0.76	0.65	0.43	0.48	0.57	0.60	0.59	0.43	0.50
Al_2O_3	15.5	17.2	9.0	9.7	16.6	22.7	19.3	14.4	19.8	13.6	19.7	14.8	15.9	15.1	11.5	8.9	10.1	11.8	10.6	10.5	9.4	10.0
Fe_2O_3	3.05	5.66	3.08	3.88	5.41	2.3	1.22	2.43	6.12	0.95	1.22	0.66	4.62	2.5	0.58	2.32	0.25	0.5	2.78	3.43	0.63	1.21
FeO	1.8	1.7	0.3	0.3	0.1	0.1	5.4	6.7	0.1	3	6.7	4.3	0.3	2.4	3.5	0.6	3.2	3.4	0.5	0.5	3	2.2
MnO	0.03	0.23	0.02	0.03	0.02	0.01	0.07	0.07	0.04	0.03	0.06	0.04	0.03	0.03	0.03	0.02	0.03	0.03	0.02	0.03	0.03	0.02
MgO	1.60	2.68	1.23	1.30	1.45	0.85	2.36	3.02	2.20	1.64	2.66	1.76	1.73	1.46	1.43	0.92	1.21	1.40	1.21	1.23	1.03	1.03
CaO	0.13	0.13	0.12	0.09	0.07	0.10	0.37	0.40	0.15	0.26	0.29	0.21	0.13	0.17	0.17	0.12	0.17	0.19	0.15	0.12	0.17	0.21
Na_2O	1.54	1.71	1.70	1.42	0.35	0.90	1.59	0.92	1.54	1.52	2.22	1.75	1.54	1.93	1.79	1.54	1.82	2.07	1.07	1.18	2.14	2.32
K_2O	2.63	3.45	1.21	1.29	2.93	4.42	3.61	2.62	3.89	2.25	3.64	2.72	2.86	2.74	1.71	1.23	1.57	1.92	1.77	1.64	1.26	1.40
P_2O_5	0.08	0.16	0.06	0.06	0.10	0.06	0.17	0.20	0.11	0.19	0.17	0.08	0.07	0.14	0.10	0.10	0.09	0.11	0.04	0.07	0.08	0.10
LOI	2.97	4.04	1.61	2.04	5.51	5.00	3.58	3.32	4.78	3.14	1.57	2.62	2.80	3.17	1.23	1.60	1.30	1.28	2.43	2.19	0.87	1.68
S	0.002	< 0.001	0.005	0.004	0.002	0.004	0.182	0.676	0.233	0.005	0.193	0.195	0.005	0.003	0.096	0.01	0.1	0.104	0.005	0.007	0.045	0.002
Total	99.8	98.6	98.9	98.2	99.9	100.8	99.4	99.6	100.7	98.2	98.2	99.2	100.9	99.6	98.4	100.8	100.7	99.1	100.9	100.1	100.2	100.3
$Fe_2O_3/(FeO+Fe_2O_3)$	0.63	0.77	0.91	0.93	0.98	0.96	0.18	0.27	0.98	0.24	0.15	0.13	0.94	0.51	0.14	0.79	0.07	0.13	0.85	0.87	0.17	0.35
AI (Alter.Index)	71.7	76.9	57.3	63.2	91.3	84.1	75.3	81.0	78.3	68.6	71.5	69.6	73.3	66.7	61.6	56.4	58.3	59.5	71.0	68.8	49.8	49.0
B	280	16	41	48	148	132	104	16	101	63	67	45	42	69	46	44	52	46	36	58	39	41
Sc	14.7	17.8	7.88	8.12	15.5	22.3	18.6	14.9	19.9	12.9	22.3	14.2	14.8	13.9	10.2	7.34	7.72	9.83	9.73	9.49	7.44	7.7
V	115	139	58	59	109	152	146	102	167	95	185	116	121	106	86	56	61	74	72	73	56	60
Cr	95.1	103	56.8	68.4	101	125	109	78.9	122	77.4	133	97.4	99.9	83.4	72.6	55.2	58.1	65.2	73	72.3	56.4	65.7
Co	5	7.1	3.6	3.9	10.8	2.4	17.6	14.3	5.7	8.2	16.4	13.9	6.4	7.4	11.5	4.5	9	9.6	4.3	9.4	8.7	8.1
Ni	25	48	14	13	29	7	60	54	22	28	67	56	19	34	36	12	30	37	24	24	30	30
Cu	19	48	14	20	36	29	35	96	34	27	70	57	32	27	21	52	19	23	9	13	24	11
Zn	104	129	82	72	130	33	129	229	104	84	164	180	93	115	81	60	83	85	127	89	67	81
As	15	27	3	2	19	3	2	2	2	3	2	16	6	4	15	5	< 1	< 1	9	5	12	6
Br	2.5	2.9	3.4	4.3	5.6	5	1	3	4.1	4	2	1.8	3.1	4.1	4.3	2.4	4.2	3.9	4.3	3.3	2	3.4
Rb	80	130	40	40	110	160	120	150	140	70	140	100	80	100	50	50	60	60	50	60	50	60
Sr	54	57	52	42	31	65	71	48	77	87	73	61	61	61	66	55	63	73	52	45	57	92
Y	24	26	21	16	19	33	30	27	32	26	33	20	23	23	19	14	16	18	18	17	14	15
Zr	203	156	167	250	208	208	193	190	198	183	188	191	209	189	199	181	232	204	204	240	174	280
Sb	0.5	0.5	0.3	2	2.9	1.1	0.6	0.8	1	0.2	0.5	0.6	0.8	0.4	0.4	0.4	0.2	0.4	0.7	0.3	0.5	0.4
Cs	29.7	6.4	5.1	8.2	20.2	13.7	18.2	30.9	17.4	6	22.4	13.1	12.2	6.8	4.3	16.5	5.7	5.6	3.7	6.8	4.1	4.8
Ba	433	812	224	246	479	720	602	327	596	450	613	403	468	477	304	189	273	319	337	290	215	217
Hf	6	5.1	4.9	6.7	6	6.6	5.4	4.8	5.8	5.4	5.3	5.4	5.8	5	5.1	5.2	5.4	5.1	5.7	6.4	4.9	7
Ta	0.9	1.2	1.1	1	0.9	1.1	1	0.9	1.2	1.1	1.1	1	1.2	< 0.3	0.8	1.3	1.1	0.8	0.6	0.9	< 0.3	1
W	< 1	< 1	3	< 1	5	6	< 1	< 1	< 1	< 1	< 1	< 1	< 1	< 1	< 1	< 1	< 1	< 1	< 1	3	< 1	< 1
Pb	5	18	17	7	11	58	17	6	19	17	17	21	14	19	10	9	10	10	106	12	10	10
Th	9	12.6	5.5	6.2	9.8	13.1	11.3	7.8	11.8	7.5	12	8.7	8.7	8.7	6.8	4.8	5.7	6.8	6.6	6.6	5.6	6
U	3.6	3.5	2.4	2.7	4.4	5.1	4.1	3.5	4.3	3.1	4.3	4.1	3.7	3.2	3.2	2.7	2.7	2.6	3.1	2.6	2.5	2.5
La	32.1	41.7	29.5	20.3	31.5	50.6	40.7	25.1	42.9	29.2	43.4	29.8	30.7	30	24.3	17.8	19.6	24.3	24.9	24.1	19.5	19.8
Ce	56	70	50	35	53	81	73	34	73	52	78	54	60	57	33	31	37	47	45	46	36	36
Nd	26	31	22	17	25	41	36	15	37	28	38	27	29	26	15	17	17	20	19	20	16	16
Sm	5.2	6	3.24	1.99	2.99	7.04	7.38	4.37	6.03	5.18	6.91	6.71	4.54	4.84	3.73	2.3	3.52	3.74	3.76	3.6	3.07	3.64
Eu	1.04	1.18	0.96	0.82	0.97	1.55	1.43	0.93	1.5	1.33	1.51	1.01	1.09	1.16	0.95	0.7	0.76	0.91	0.91	0.84	0.71	0.79
Tb	1	1	< 0.1	0.9	0.6	1.7	0.9	1	1.2	0.5	1.5	0.6	0.7	1	0.8	0.5	< 0.1	0.6	0.7	0.6	0.7	< 0.1
Yb	2.72	3.18	1.84	1.88	2.47	3.61	3.19	2.54	3.51	2.61	3.67	2.62	2.74	2.59	2.26	1.55	1.86	2.21	2.07	2.11	1.79	1.84
Lu	0.42	0.5	0.3	0.3	0.39	0.55	0.54	0.44	0.52	0.41	0.64	0.44	0.47	0.43	0.37	0.26	0.32	0.38	0.31	0.34	0.29	0.3
REE total	124.5	154.6	107.8	78.2	116.9	187.1	163.1	83.4	165.7	119.2	173.6	122.2	129.2	123.0	80.4	71.1	80.1	99.1	96.7	97.6	78.1	78.4
$\delta^{18}O_{V\text{-}SMOW}$ (‰)	13.8	10.6	15.6	16.6	16.4	15.7	13.6	13.4	13.4	14.8	12.4	13.2	13.2	14.7	15.1	14.5	15.4	15.4	15.9	14.6	15.2	15.2

Elements below detection limits or present in very low concentrations were not included in this Table (e.g., F ≤ 0.05%, Be ≤ 3 ppm)

though field observations and some geochemical data show that phyllosilicate-rich spotted-schists and metapelites tend to be more affected by weathering than quartz-richer rocks, such as hornfelses, metapsammites and metagreywackes.

Trace components such as Ba, Rb, Ti, Cr, Sc and the REE are preferentially accommodated in the phyllosilicate minerals, and show very good positive correlation with whole-rock Al_2O_3 (Table 1; Figs. 2c and 3b). Concentrations of these elements are invariably higher in spotted-schists and regional metapelites than in hornfelses and regional metagreywackes.

In spite of their distinct total REE contents (< 100 ppm in hornfelses, 117-187 ppm in spotted-schists, and 124–155 ppm in regional metapelites; Table 1; Fig. 2d), chondrite-normalized LREE-enriched patterns for the P–M spotted-schists (Fig. 4a) and hornfelses (Fig. 4b) are similar in shape and match, respectively, the general REE patterns of SGC metapelites and metapsammites/metagreywackes of Late Precambrian and Ordovician age (data from Beetsma 1995). This close similarity with the REE patterns of regional metasediments implies there is no significant variation of these elements during thermal metamorphism. Besides, the trace-element composition, namely the REE, Y and Zr contents, of the P–M regional and contact-zone rocks (Fig. 4c) show systematic depletion relative to the Neoproterozoic Iberian Average Shale composition (NIBAS, Ugidos et al. 2010), matching the geochemical features of the southern terrane of the CIZ (Villaseca et al. 2014).

Oxygen isotope data for the studied contact rocks show some variation (Table 1), with $\delta^{18}O$ values ranging from 14.5 to 15.9‰ for hornfelses and from 12.4 to 16.4‰ for spotted-schists, as compared with 10.6–16.6‰ for the regional metasediments sampled outside the contact zone. This oxygen isotope heterogeneity within the metasedimentary host-rocks seems to be in line with their geochemical and mineralogical heterogeneity, though previous studies (e.g., Vindel et al. 2014) yielded relatively homogeneous $\delta^{18}O$ values (13.1–13.4‰) for some Neoproterozoic SGC metasediments. The unusually low value obtained for sample P-14 (10.6‰) is probably due to the low quartz contents and considerable amount of Fe-oxyhydroxides in this regional metasediment compared to the other samples.

4.2 Contact aureole: mineral chemistry

Representative and average compositions of the essential minerals in the spotted-schists and hornfelses from the P-M contact zone are given in Tables 2, 3, 4, 5 and 6, and compared with those from the neighbouring country rocks.

Plagioclase, with compositions $An_{0.4–11.7}$ (Table 2), is relatively abundant in hornfelses, but rare in the spotted-schists, where $An_{0.8–7.0}$ compositions were obtained. K-feldspar (microcline) was only identified occasionally in hornfelses.

Given the predominant metapelitic character of the country rocks, both spotted-schists and hornfelses contain significant, though highly variable, amounts of micas and chlorite, all of which show some Fe–Mg substitution, but limited Tschermak [$Al^{VI}\,Al^{IV} \rightarrow (Fe + Mg)^{VI}\,Si^{IV}$] substitution (Figs. 5a, b and 6b).

Muscovite in the P–M host-rocks and a few spotted-schists is typical low-temperature phengite, with up to 0.51–0.60 (Mg + Fe) *apfu* replacing Al^{VI} (Table 3; Fig. 5a), but compositions tend to be more aluminous in most spotted-schists and, particularly, in the hornfelses, where more than 70% of the analysed muscovite exhibit only 0.07-0.12 $(Mg + Fe)^{VI}$ *apfu*, as expected in higher grade muscovite, where the extent of phengitic substitution decreases as biotite begins to form (Ernst 1963; Miyashiro 1978, 1994). While Mg/(Fe + Mg) ratios in the analysed muscovite crystals are quite variable in both regional host-rocks (0.34–0.62) and contact rocks (0.30–0.68), and do not seem to correlate with metamorphic grade (Table 3), the $(Fe + Mg)/(Al + Fe + Mg)^{VI}$ ratios are markedly lower for most contact rocks (Figs. 5b and 7). On the contrary, muscovite from contact rocks tends to display higher Al^{IV} and Na contents than muscovite from host metasediments (Fig. 5b, c; Table 3).

As often happens in metapelites (e.g., Evans and Guidotti 1966), the Mg/(Mg + Fe) ratios of coexisting muscovite and biotite show sympathetic variation (Fig. 6a), indicating that both minerals are close to chemical equilibrium in these contact-zone rocks.

Chlorite and biotite are the main ferro-magnesian minerals in the P–M regional metapelites and in the contact-zone rocks; relic cordierite appears only in a few samples.

Chlorite from the P–M contact rocks exhibits limited $Si^{IV}(Mg,Fe^{2+})^{VI} = Al^{IV}Al^{VI}$ substitution, with 2.57–2.99 Si *apfu* (Table 4; Fig. 6b), as is typical in metapelites (Miyashiro 1978), as well as little variation in the proportions of octahedral Al (1.44 – 1.64 *apfu*) and Mg/(Fe + Mg) ratios (0.44–0.49 in spotted-schists; 0.43–0.48 in hornfelses, and 0.43–0.49 in the host metasediments; Table 4). Chlorite H_2O contents, estimated by difference of analysed compositions to 100 wt%, tend to decrease slightly from regional metasediments (10.1–17.7 wt%) to spotted-schists (8.9–14.9 wt%) and hornfelses (9.1–12.9 wt%).

Biotite in the three rock types considered also shows remarkable constancy in its octahedral Al proportions (0.42–0.62 *apfu*) and Mg/(Fe + Mg) ratios (0.35–0.47) (Table 5; Fig. 6b, c). As expected (e.g., Miyashiro 1978), crystallization of biotite in the contact-rocks tends to lower the Fe^{2+}/Mg ratios in associated chlorite (Tables 3 and 4). Moreover, Ti contents tend to increase as biotite progressively replaces chlorite in the P–M contact rocks (0.11–0.20 *apfu*; Table 5; Fig. 6c), compared to those in biotite from regional metapelites (0.10), which means, according to

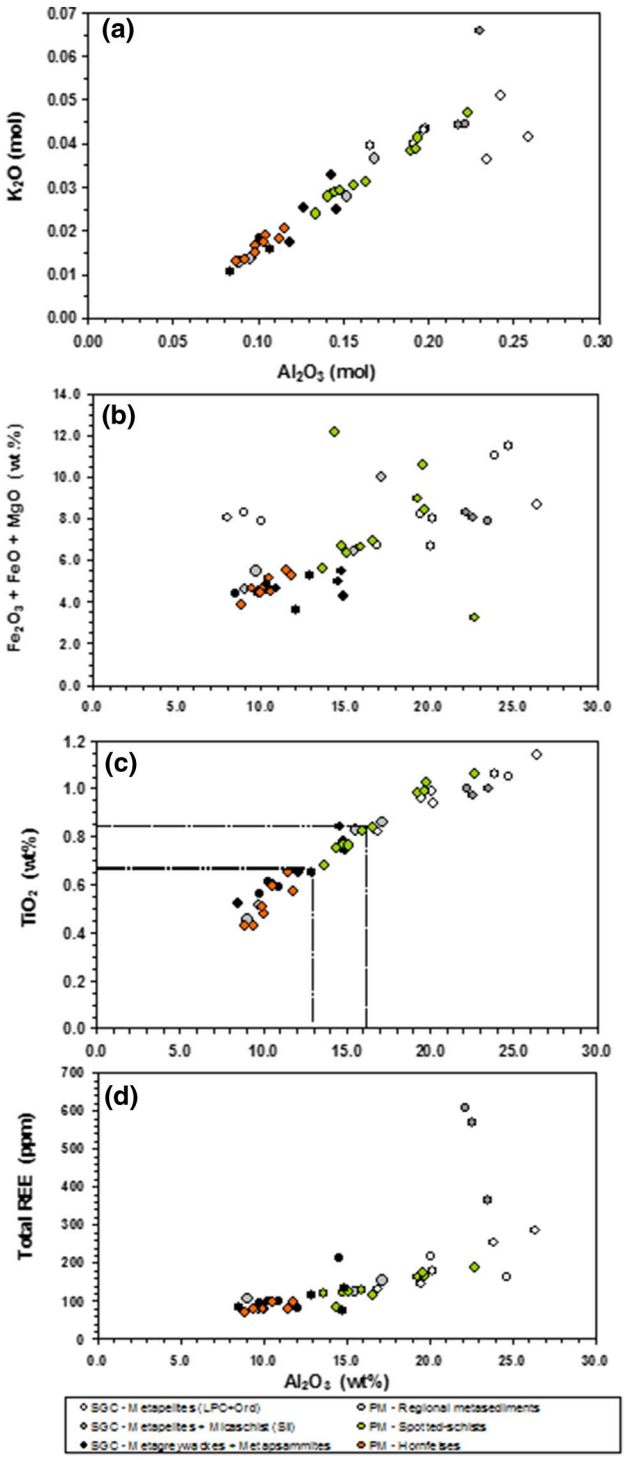

Fig. 2 Geochemical data of the sampled regional and contact-zone rocks surrounding the Penamacor–Monsanto granite pluton, set against data for SGC metasedimentary rocks of Late Precambrian, Ordovician and Silurian age (Beetsma 1995): **a** K_2O (mol) vs Al_2O_3 (mol); **b** Fe_2O_3/(FeO + Fe_2O_3) vs Al_2O_3 (wt%); **c** TiO_2 (wt%) vs Al_2O_3 (wt%); **d** Total REE (ppm) vs Al_2O_3 (wt%)

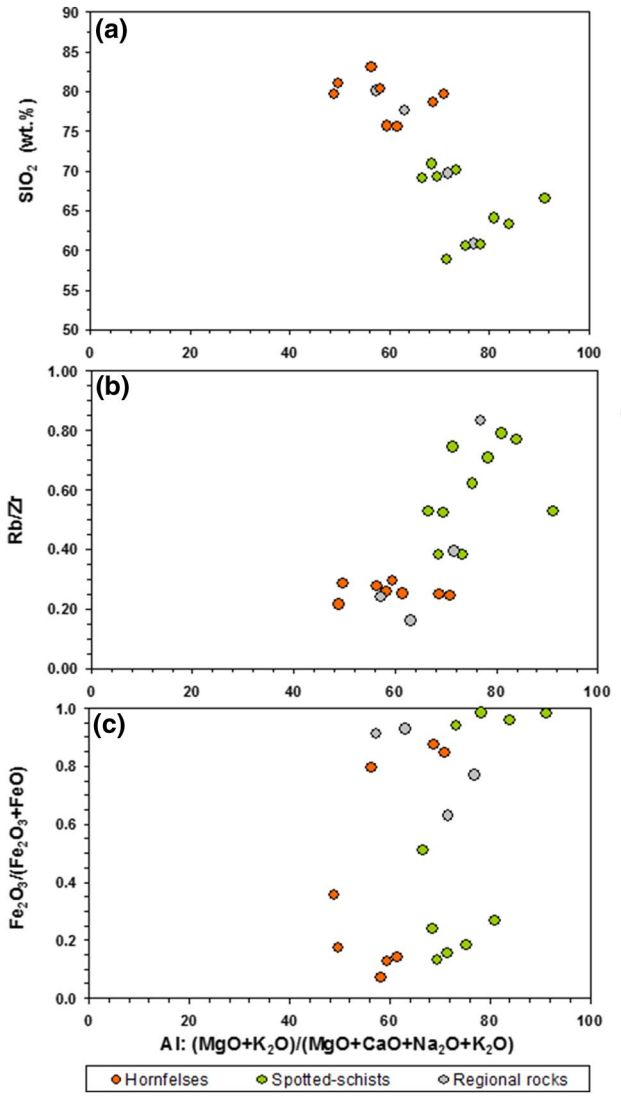

Fig. 3 Correlations between bulk-rock **a** SiO_2, **b** Rb/Zr and **c** Fe_2O_3/(FeO + Fe_2O_3) ratios and the alteration index (AI; Ishikawa et al. 1976) for the contact-zone and nearby regional rocks surrounding the Penamacor–Monsanto pluton

Miyashiro (1994), enhanced stability of biotite in the contact rocks.

Intermediate compositions corresponding to the chlorite - biotite transition were included in Table 5, to document the progressive enrichment in K_2O (0.77–5.99 wt%), TiO_2 (0.09–2.55 wt%), and occasionally in SiO_2, as dehydration proceeds and chlorite gives way to biotite in the contact-zone rocks.

Relic cordierite porphyroblasts are found only in a few spotted-schists and are rare in hornfelses (e.g., sample P-36A). Total Al contents in these cordierite relics are quite similar (0.97–1.03 Al^{IV}*apfu* in spotted-schists and 0.91-1.02 Al^{IV}*apfu* in hornfels; 60–62% Al^{VI} in both rock types; Table 6), and their Mg/(Fe + Mg) ratios are

typical of metamorphic cordierite (> 0.40, Miyashiro 1978), though they tend to be slightly higher in cordierite relics from hornfelses (0.53–0.60) than in those from spotted-schists (0.49–0.60). Weathered ghost cordierite porphyroblasts, on the other hand, are ubiquitous in the spotted-schists, recognized by their oval-shape and abundant quartz and sericite micro-inclusions (cf. Pattison and Tracy 1991; Vernon and Clarke 2008). X-ray mapping of key elements revealed that concentric zonation displayed by some ghost cordierite porphyroblasts is due to grain-size heterogeneities of precursor minerals from the rock matrix (quartz and mica, mostly), rather than to compositional variations.

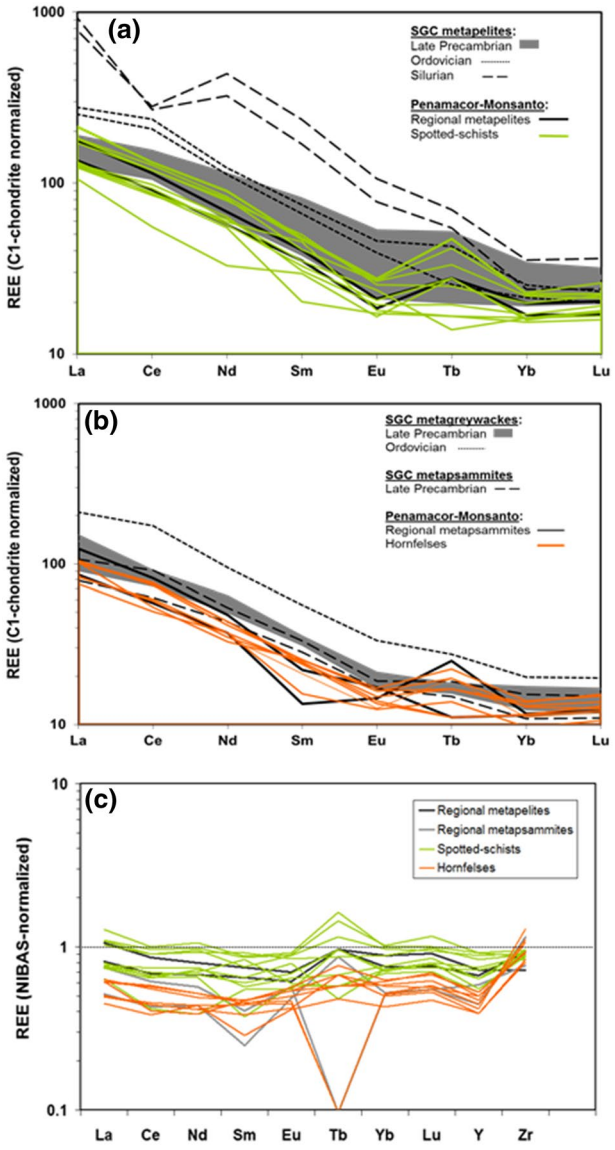

Fig. 4 Comparison of chondrite-normalized REE patterns for the Penamacor–Monsanto contact- and host-rocks with those of SGC metasediments (data from Beetsma 1995): **a** P–M regional metapelites and contact-zone spotted-schists, against SGC metapelitic rocks of late Precambrian, Ordovician and Silurian age; **b** P-M regional metapsammites and contact-zone hornfelses, against SGC metapsammites and metagreywackes of late Precambrian and Ordovician age; **c** REE-Y-Zr patterns of P–M regional and contact-zone rocks, normalized to the NIBAS composition (NIBAS data from Ugidos et al. 2010)

The Mg–Fe distribution in the coexisting ferromagnesian minerals (Chl + Bt ± Crd) of the P–M contact-zone rocks follows a typical trend (e.g. Thompson 1976; Miyashiro 1978, 1994), with Mg/(Mg + Fe) ratios in Bt < Chl < Crd (Fig. 7). This diagram also confirms that muscovite displays higher Mg/(Mg + Fe) ratios than coexisting chlorite (cf. Miyashiro 1978).

5 Discussion

5.1 Contact metamorphic parageneses

Spotted-schists and occasional hornfelses make up the P–M contact aureole. Frequently described in metapelitic-hosted contact zones (e.g. Miyashiro 1978), field and petrographic distinction between spotted-slates and spotted-schists is tenuous at best in this aureole. Following porphyroblast-size criteria (cf. Miyashiro 1978), all P–M porphyroblast-bearing contact-rocks exhibiting clear foliation have been considered spotted-schists.

The parageneses of the P–M contact–zone rocks include Ms + Chl + Bt (mineral name abbreviations according to Whitney and Evans 2010), indicating that thermal metamorphic crystallization must have begun at temperatures where both chlorite and biotite were stable (Miyashiro 1994). The biotite-producing reaction Chl + Ms ± Kfs = Bt + Ms + Qz + H_2O may proceed continuously over a range of temperatures (Miyashiro 1994). In the *biotite zone*, then, typical metapelites show the Bt + Chl assemblage accompanied by Ms, Qz and Ab. In the P–M contact rocks, however, the expected increase of the Mg/(Mg + Fe) ratios of coexisting chlorite and biotite, with increasing temperature, is not observed.

The appearance of cordierite is the result of prograde dehydration reactions, closer to the intrusion, such as: Ms + Chl + Qz = Crd + Bt + H_2O (Pattison and Tracy 1991; Miyashiro 1994). K-feldspar, though not very abundant, occurs in the P–M hornfels and may have formed at the same time as cordierite: Ms + Phl + Qz = Mg–Crd + Kfs + H_2O (cf. Pattison 1987).

5.2 Thermal conditions

Textural, mineralogical, geochemical and isotopic features of the P–M contact rocks have been used to estimate the approximate peak metamorphic temperatures affecting the

Table 2 Representative EMP data and structural formulae for plagioclase from the spotted-schists and hornfelses of the Penamacor–Monsanto contact zone

	Plagioclase in spotted-schists (5 an.)				Plagioclase in hornfelses (28 an.)			
	An. 1	An. 2	Average	Std. Dev.	An. 1	An. 2	Average	Std. Dev.
SiO_2	69.24	66.48	68.49	1.35	69.15	66.33	68.69	1.11
TiO_2	0.01	–	0.00	0.00	0.04	0.01	0.01	0.04
P_2O_5	0.01	0.42	0.09	0.19	0.09	–	0.01	0.03
Al_2O_3	20.62	21.62	20.65	0.67	19.6	21.53	20.10	0.75
FeO	–	0.32	0.10	0.13	0.06	0.12	0.09	0.06
BaO	–	0.10	0.04	0.05	0.04	0.06	0.06	0.03
CaO	0.17	1.46	0.50	0.55	0.09	2.40	0.51	0.53
Na_2O	11.18	10.72	10.84	0.64	11.16	9.99	10.98	0.32
K_2O	0.04	0.08	0.04	0.03	0.03	0.04	0.04	0.02
Total	101.28	101.38	100.79	0.89	100.26	100.63	100.54	1.07
Cations calculated on a basis of 8 oxygen atoms								
Si	2.978	2.884	2.964	0.045	3.003	2.896	2.982	0.035
Al	1.045	1.106	1.053	0.031	1.003	1.108	1.028	0.037
P	0.000	0.015	0.003	0.007	0.003	0.000	0.001	0.001
Ti	0.000	0.000	0.000	0.000	0.001	0.000	0.000	0.001
Fe^{2+}	0.000	0.012	0.004	0.005	0.002	0.004	0.003	0.002
Ba	0.000	0.002	0.001	0.001	0.001	0.001	0.001	0.001
Ca	0.008	0.068	0.023	0.025	0.004	0.112	0.024	0.025
Na	0.932	0.902	0.910	0.059	0.940	0.846	0.924	0.025
K	0.002	0.005	0.002	0.002	0.002	0.002	0.002	0.001
Total cation	4.966	4.993	4.960	0.044	4.960	4.974	4.966	0.014
(%An)	0.84	6.97	2.48	2.60	0.44	11.69	2.48	2.56

host SGC rocks during the emplacement of the granitic pluton.

As referred above, most of the regional SGC metasediments are mica-rich and belong to the *chlorite zone* (e.g. Oen 1970, Gama Pereira 1976), though petrographic evidence suggests they may occasionally reach the *biotite zone*. The composition of detrital tourmaline in these regional metasediments, namely its Mg/(Mg + Fe) = 0.4–0.7, high vacancy concentration in the A position and low F and Al^{IV} contents (Ribeiro da Costa et al. 2014), also restricts them to medium-grade metamorphism (cf. Henry and Dutrow 1996).

The P–M contact aureole conforms to the general model for contact metamorphism in metapelitic rocks (cf. Miyashiro, 1978, 1994), showing an outermost aureole characterized by the coexistence of Ms + Chl + Bt, defining a thermal zone where both biotite and chlorite are stable, and progressive metamorphic crystallization towards the intrusion, marked by the appearance of cordierite in the inner zone.

Albitic plagioclase predominates in both spotted-schists and hornfelses (Table 2), as expected in low- and medium-grade metapelites (prehnite-pumpellyite to greenschist facies; Miyashiro 1978), though the occasional occurrence of oligoclase in a few hornfelses suggests local transition towards the amphibolite facies (cf. Miyashiro 1978). The K-feldspar identified in a few P–M hornfelses also points to temperatures corresponding to the greenschist-amphibolite transition, below muscovite breakdown reactions (cf. Miyashiro 1978).

Departure from ideal muscovite composition is also a good indicator of metamorphic temperature (e.g., Miyashiro 1978). Phengitic compositions (with up to 20–25% celadonitic component) are stable below ~ 400 °C, therefore typical in the low- and medium-grade SGC host-rocks and in a few P–M spotted-schists. On the other hand, Al-richer compositions closer to ideal muscovite (with 4–6% celadonitic component) occur in the P–M hornfelses and in most of the spotted-schists (Figs. 5a and 8), indicating increasing metamorphic grade, though temperatures may have not exceeded the lower limit of the amphibolite facies. Spotted-schists containing phengitic muscovite correspond to the most weathered contact-zone samples (P-16 and P-18), so muscovite composition may have been retrograded.

As muscovite and chlorite have higher Mg/Fe^{2+} ratios than coexisting biotite, the progress of biotite-producing reactions in low-P metapelites tends to increase the Mg/Fe^{2+} ratio in biotite, unless cordierite begins to form (Miyashiro 1978). The fact that Mg/(Mg + Fe) ratios in biotite do not seem to vary much in the studied rocks may indicate that temperatures along the granite border were not high enough to promote more extensive crystallization of cordierite.

Cordierite porphyroblasts occur in most spotted-schists and a few hornfelses of the P–M and other contact aureoles

Table 3 Representative EMP data and structural formulae for muscovite from the regional metasediments and from the spotted-schists and hornfelses of the Penamacor–Monsanto contact aureole

	Regional rocks (5 an.)				Spotted-schists (22 an.)				Hornfelses (34 an.)			
	An. 1	An. 2	Average	Std. Dev.	An. 1	An. 2	Average	Std. Dev.	An. 1	An. 2	Average	Std. Dev.
SiO_2	51.00	47.54	49.14	1.41	55.72	46.49	47.99	2.57	47.72	46.23	46.97	0.81
TiO_2	0.54	0.16	0.39	0.19	0.11	0.58	0.40	0.27	0.67	0.52	0.59	0.27
Al_2O_3	30.91	35.96	32.48	3.11	31.77	37.07	35.94	2.24	31.81	38.14	36.15	1.59
FeO	2.63	1.80	3.30	1.30	1.67	1.07	1.44	1.18	2.27	0.77	1.06	0.45
MnO	0.14	0.06	0.10	0.06	0.00	0.00	0.02	0.03	0.03	0.00	0.03	0.03
MgO	2.45	0.89	1.83	0.89	2.03	0.59	0.87	0.80	1.68	0.49	0.76	0.41
BaO	0.39	0.13	0.27	0.12	0.28	0.11	0.23	0.10	0.08	0.21	0.19	0.11
CaO	0.00	0.02	0.01	0.01	0.00	0.04	0.03	0.04	0.00	0.08	0.00	0.02
Na_2O	0.14	0.27	0.19	0.07	0.48	0.67	0.67	0.34	0.32	0.83	0.67	0.13
K_2O	10.04	8.81	9.30	0.98	6.04	9.91	8.43	1.26	10.06	9.69	9.63	0.39
Rb_2O	0.00	0.00	0.02	0.03	0.00	0.02	0.01	0.02	0.21	0.02	0.04	0.07
F	0.08	0.00	0.03	0.04	0.05	–	< 0.05	–	1.20	–	0.59	0.53
Total	98.32	95.70	97.08	1.35	98.18	96.56	96.15	1.61	96.06	97.05	96.33	1.24
Cations per formula unit, on a basis of 11 oxygen atoms												
Si	3.298	3.118	3.216	0.085	3.470	3.040	3.125	0.109	3.202	3.005	3.081	0.047
Al^{IV}	0.702	0.882	0.784	0.085	0.530	0.960	0.875	0.109	0.798	0.995	0.919	0.047
Al^{VI}	1.653	1.897	1.720	0.154	1.802	1.897	1.885	0.091	1.717	1.927	1.875	0.067
Ti	0.026	0.008	0.019	0.009	0.005	0.029	0.020	0.013	0.034	0.025	0.029	0.014
Fe	0.142	0.099	0.181	0.072	0.087	0.059	0.079	0.067	0.127	0.042	0.058	0.025
Mn	0.007	0.003	0.006	0.003	0.000	0.000	0.001	0.002	0.002	0.000	0.001	0.002
Mg	0.236	0.087	0.179	0.088	0.188	0.057	0.084	0.079	0.168	0.048	0.074	0.041
Ba	0.010	0.003	0.007	0.003	0.007	0.003	0.006	0.003	0.002	0.005	0.005	0.003
Ca	0.000	0.001	0.000	0.001	0.000	0.003	0.002	0.003	0.000	0.006	0.000	0.001
Na	0.018	0.034	0.024	0.009	0.058	0.085	0.085	0.043	0.041	0.105	0.085	0.016
K	0.828	0.737	0.776	0.080	0.480	0.827	0.703	0.115	0.861	0.804	0.806	0.034
Rb	0.000	0.000	0.001	0.001	0.000	0.001	0.001	0.001	0.009	0.001	0.002	0.003
Total	6.921	6.870	6.913	0.062	6.628	6.959	6.869	0.107	6.962	6.963	6.939	0.027
$(Fe + Mg)/(Al^{VI} + Fe + Mg)$	0.19	0.09	0.17	0.07	0.13	0.06	0.08	0.06	0.15	0.04	0.07	0.03

The muscovite analyses presented cover the Al^{IV} range obtained for each rock type

in this region (Gama Pereira 1976). The appearance of cordierite is expected in low-P (≤ 4 kbar) metapelitic assemblages of low-intermediate metamorphic grade (< 450 to 450–650 °C), on the high-T side of the biotite isograd (Miyashiro 1978). Indeed, even in highly aluminous protoliths, andaluzite is usually absent until muscovite and quartz disappear completely (Pattison and Tracy 1991). Notwithstanding the effects of advanced weathering and occasional retrogradation of the spotted-schists, the grainsize-related zonation in some ghost cordierite porphyroblasts (as in samples P-16 and P-18; Ribeiro da Costa et al. 2013), the abundance of micro-inclusions (suggesting fast initial growth) and the similarity between micro-inclusion mineralogy and that of the surrounding matrix reinforce the idea that the thermal effects of granite emplacement may have been relatively weak in several places of the exocontact, thus inhibiting full development of porphyroblasts.

Although Miyashiro (1994) and other authors predict that MgO/FeO ratios in ferromagnesian minerals should increase with increasing temperature, this trend is not evident in the P–M contact rock minerals. Moreover, cordierite and biotite from the P–M contact-zone rocks show considerable compositional homogeneity and the Mg–Fe distribution coefficient between these two coexisting, unzoned minerals (cf. Pattison 1987) does not show significant variation: $K^{Crd-Bt}_{D(Mg-Fe)} = 1.40$ in one spotted-schist, and varies between 1.41 and 1.43 in four hornfelses. This similarity also favours the hypothesis that the P–M spotted-schists and hornfelses do not represent

Table 4 Representative EMP data and structural formulae for chlorite from the regional metasediments and from the spotted-schists and hornfelses of the Penamacor–Monsanto contact zone

	Chlorites in regional host-rocks (9 an.)				Chlorites in spotted-schists (6 an.)				Chlorites in hornfelses (7 an.)			
	An.1	An. 2	Average	Std. Dev.	An.1	An. 2	Average	Std. Dev.	An.1	An. 2	Average	Std. Dev.
SiO_2	26.35	27.67	26.88	1.08	25.87	26.73	26.25	1.24	24.77	24.63	25.67	1.73
TiO_2	0.19	0.06	0.13	0.08	0.08	0.60	0.31	0.24	0.15	0.20	0.12	0.13
Al_2O_3	21.15	21.98	22.19	1.14	22.38	20.62	22.10	1.03	23.97	23.37	23.38	0.56
FeO	27.74	24.33	25.37	1.25	28.89	25.12	26.26	1.84	27.64	25.46	26.60	1.42
MnO	0.09	0.93	0.36	0.35	0.22	0.07	0.15	0.09	0.36	0.04	0.19	0.10
MgO	11.55	12.89	12.63	0.55	12.57	11.08	12.25	0.82	11.72	12.93	12.51	0.73
ZnO	0.00	0.03	0.07	0.14	–	–	0.01	0.02	0.29	0.21	0.14	0.12
BaO	0.06	0.13	0.09	0.05	0.05	–	0.05	0.05	0.12	0.08	0.07	0.05
CaO	0.24	0.03	0.08	0.08	0.01	–	0.01	0.02	0.03	0.04	0.05	0.04
Na_2O	0.04	0.00	0.03	0.04	–	–	0.01	0.01	–	–	0.01	0.02
K_2O	0.31	0.39	0.24	0.29	0.00	0.75	0.47	0.62	0	0.00	0.11	0.29
F	0.00	0.00	0.00	0.00	–	–	0.00	0.00	–	–	0.00	0.00
Total	88.41	88.46	88.18	1.54	90.13	85.07	87.92	2.74	89.08	87.01	88.93	1.42
Cations per formula unit, on a basis of 14 oxygen atoms												
Si	2.808	2.870	2.811	0.086	2.692	2.904	2.769	0.106	2.601	2.618	2.677	0.144
Al^{IV}	1.192	1.130	1.189	0.086	1.308	1.096	1.231	0.106	1.399	1.382	1.323	0.144
Al^{VI}	1.464	1.557	1.545	0.083	1.437	1.544	1.518	0.080	1.567	1.546	1.552	0.076
Ti	0.015	0.005	0.010	0.007	0.006	0.049	0.025	0.020	0.012	0.016	0.010	0.010
Fe	2.472	2.110	2.220	0.132	2.514	2.282	2.315	0.121	2.427	2.264	2.323	0.136
Mn	0.009	0.081	0.032	0.031	0.020	0.006	0.013	0.008	0.032	0.004	0.017	0.009
Mg	1.834	1.992	1.968	0.087	1.949	1.794	1.925	0.113	1.834	2.048	1.947	0.124
Zn	0.000	0.002	0.006	0.011	0.000	0.000	0.001	0.001	0.022	0.016	0.011	0.010
Ba	0.003	0.005	0.004	0.002	0.002	0.000	0.002	0.002	0.005	0.003	0.003	0.002
Ca	0.027	0.003	0.009	0.009	0.002	0.000	0.002	0.002	0.004	0.004	0.005	0.004
Na	0.008	0.000	0.006	0.007	0.000	0.000	0.001	0.002	0.000	0.000	0.002	0.003
K	0.041	0.052	0.031	0.038	0.000	0.104	0.063	0.082	0.000	0.000	0.014	0.037
Total	9.873	9.808	9.831	0.048	9.929	9.779	9.864	0.052	9.904	9.902	9.884	0.096
Mg/(Mg + Fe)	0.43	0.49	0.47	0.02	0.44	0.44	0.45	0.02	0.43	0.48	0.46	0.02
T (°C)	321.9	301.9	321.0	27.6	359.2	291.0	334.6	34.2	388.5	383.0	381.0	46.2

The chlorite analyses presented cover the Mg/(Mg + Fe) range obtained for each rock type. Crystallization temperatures are given below and were obtained using the chlorite geothermometer of Cathelineau (1988)

progressive metamorphic temperature ranges, but are instead the result of contact metamorphism on two distinct metasedimentary facies, namely pelitic and psammitic.

The Cathelineau (1988) chlorite geothermometer, based on the amount of tetrahedral Al in the chlorite structure, indicates a general trend of increasing metamorphic temperatures from the host metasediments (261–351 °C; av. 321 ± 28 °C) to the spotted-schists (291–368 °C; av. 335 ± 34 °C) and hornfelses (370–398 °C; av. 381 ± 19 °C) (Fig. 9a). Moreover, octahedral vacancies in the chlorite structure are also affected by temperature and tend to decrease in the contact-rock chlorites as temperature increases (Fig. 9b), as shown in previous studies (e.g. De Caritat et al. 1993).

On the other hand, the geothermometers proposed by Henry and Guidotti (2002) and by Henry et al. (2005), based on the Ti contents and Mg/(Mg + Fe) ratios of metamorphic biotites in metapelitic rocks, yield temperatures in the order of 577–589 °C (regional metasediments), 585–687 °C (spotted-schists) and 433–694 °C (hornfelses) (Fig. 10), which are too high for the local metamorphic conditions and are not compatible with other evidence for this contact zone. Possible causes for this overestimation may be that both regional and contact-zone rocks formed at very low-pressure (≤ 4 kbar; Gama Pereira 1976), much below the 4–6 kbar range for which this geothermometer was established, and/or that P–M biotites may contain higher Ti than most metapelite biotites.

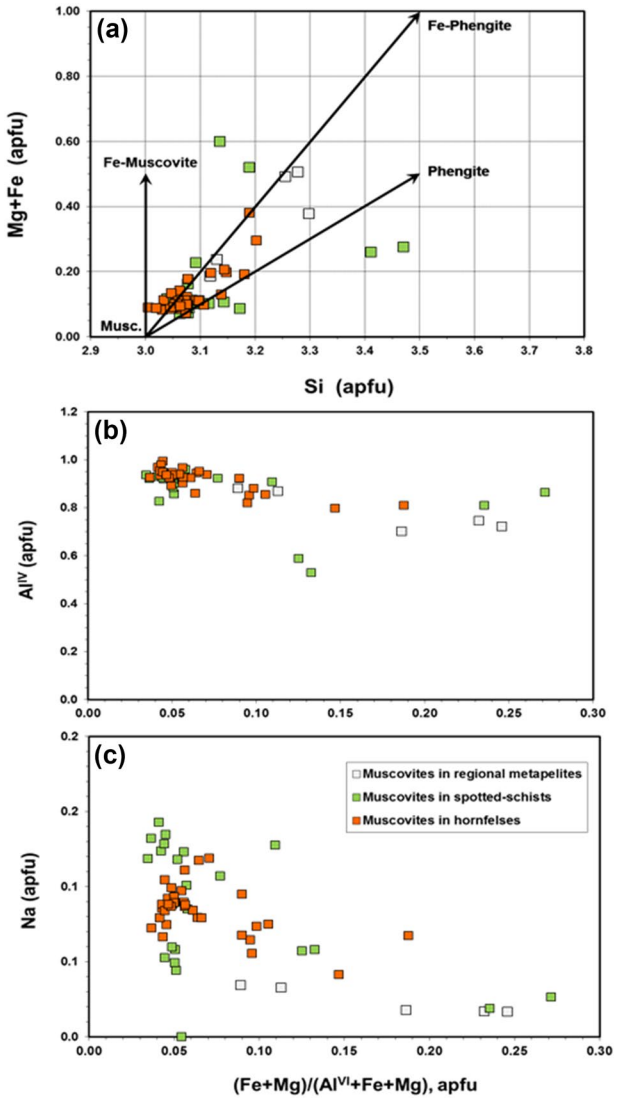

Fig. 5 Muscovite characterization: **a** (Mg + Fe) vs. Si diagram showing muscovite – phengite trends; correlations between Al^{IV} (**b**) and Na (**c**) and (Mg + Fe)/(Al^{VI} + Mg + Fe) in the muscovites from Penamacor–Monsanto aureole and host-rocks

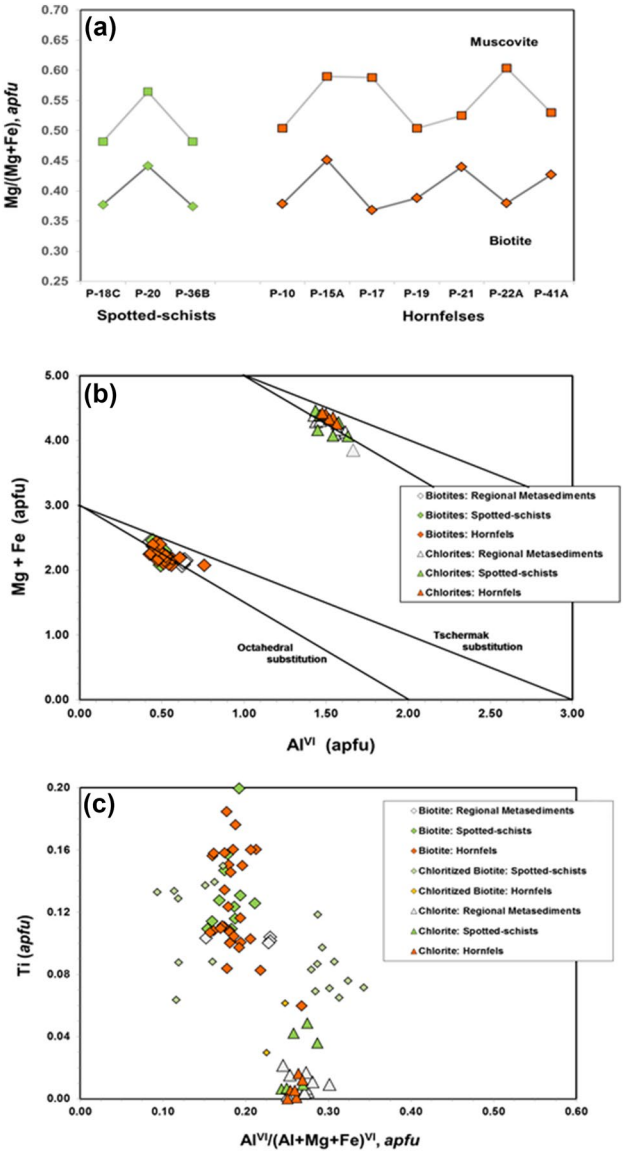

Fig. 6 **a** (Mg/(Mg + Fe) covariation in muscovites from the spotted-schists and hornfelses of the Penamacor–Monsanto contact zone; **b** (Mg + Fe) vs. Al^{VI} diagram showing trends for octaehedral and Tschermak substitutions in chlorites and biotites from the Penamacor–Monsanto contact and host rocks; **c** negative correlation between Ti and octahedral Al in the whole chlorite–biotite range from the Penamacor–Monsanto contact aureole and host-rocks

Garnet is absent in the P–M metamorphic aureole, well in keeping with the very low MnO molar contents of these rocks (0.0001–0.001; Table 1). Nevertheless, using bulk-rock [MnO]/[FeO + MnO + MgO] ratios to predict the lowest temperature at which garnet might occur at the low pressure characteristic of thermal metamorphism (Miyashiro 1994), it was possible to infer that temperatures at the P–M contact aureole have not reached 515–507 °C. This would mean that thermal metamorphism has not exceeded the lower limit of the amphibolite facies, which is in good agreement with the oxygen isotope-based temperatures for granite emplacement (Ribeiro da Costa et al. 2014) and with the mineralogical data presented above.

Bulk-rock molar MgO/(MgO + FeO) ratios for the P–M host metapelites vary between 0.32 and 0.42, largely within the limited range (0.35–0.55) established for most low-T metapelitic rocks (e.g., Miyashiro 1994), and plot in the field between the almandine-chlorite line and the biotite line in the AFM diagram (Thompson 1976).

Thermal metamorphism related to the P–M intrusion seems to have been essentially isochemical, with bulk-rock geochemistry essentially controlled by pre-existing SGC heterogeneities (Table 1): high-alumina spotted-schists are

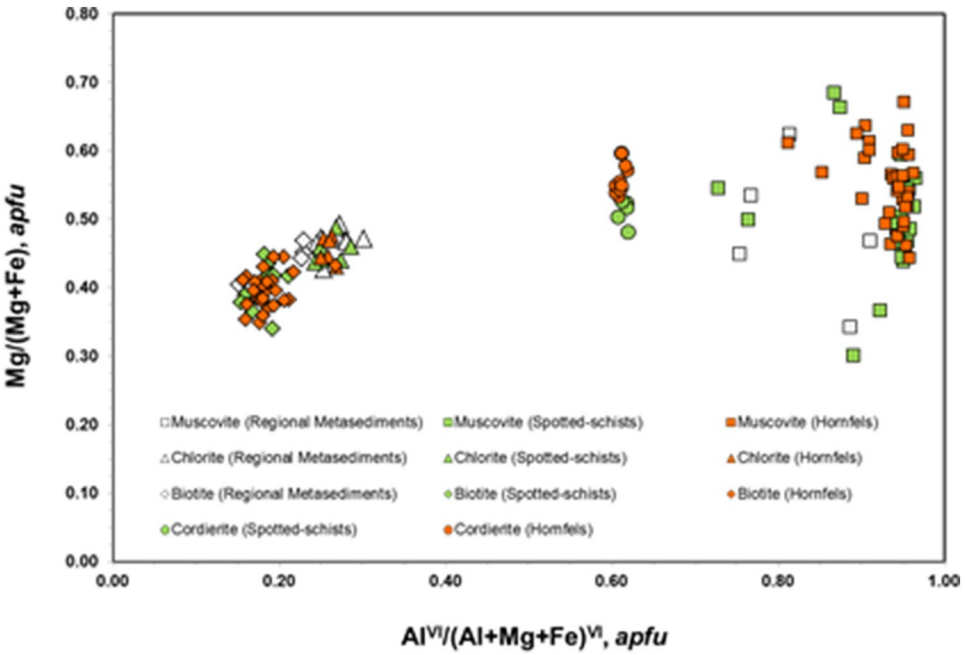

Fig. 7 Relative co-variation of Mg/(Mg + Fe) vs. Al^{VI}/(Al^{VI} + Mg + Fe) for muscovites and Fe–Mg minerals from the Penamacor–Monsanto contact zone and host-rocks

compositionally close to the ubiquitous regional metapelites, whereas the high silica and lower K_2O, Rb, Ba and REE contents that characterize hornfelses replicate the bulk composition of the localized siliciclastic/psammitic facies within the SGC.

Oxygen isotopes can be good tracers for studying thermal responses of wall-rocks to the emplacement of hot magmas and provide valuable evidence for diffusional processes in contact metamorphic minerals and for fluid-rock interaction accompanying the emplacement of hot intrusions in the upper crust (Taylor 1974; Sheppard 1986; Nabelek 1991).

Oxygen isotope values obtained for contact rocks from the P–M metamorphic aureole are wide-ranging ($\delta^{18}O$ = 12.4–16.4‰; Table 1), but fall within the intervals established for the host SGC metasediments (10.6–16.6‰) and for diagenetic rocks of pelitic nature (~ 14–19‰, Savin and Epstein 1970). While these values do not show any obvious effects of isotopic exchange between the host metasediments and the magmatic intrusion (Fig. 11), and are therefore of little use in distinguishing the specific effects of contact metamorphism from those of previous regional-scale metamorphism, they imply nonetheless that thermal metamorphic reactions related to the P–M intrusion have occurred essentially in the absence of magmatic fluids.

Moreover, and unlike the trends observed in other metamorphic aureoles, such as in the argillites hosting the Notch Peak intrusion (Utah) or in the contact schists of the Birch Creek granite (California), where $\delta^{18}O$ values reequilibrate and decrease with increasing metamorphic grade, approaching the isotopic composition of the intrusion (Shieh and Taylor 1969), no perceptible distinction has been found between the oxygen isotopic signatures of the P–M hornfelses and spotted-schists, which values overlap considerably, irrespective of the relative distance from the pluton (Fig. 11). Together with the fact that $\delta^{18}O$ values for the contact rocks are similar to those of regional metasediments, this implies that not much isotopic exchange has occurred across the P-M metasediment—granite contact, suggesting that (i) apart from the late B-rich magmatic fluids responsible for exocontact tourmalinization (Ribeiro da Costa et al. 2014), little magmatic fluid intervened in the thermal metamorphism of the host rocks, and (ii) this may be a "closed" aureole, in the sense that it shows little or no intervention of infiltrated meteoric water (cf. Nabelek 1991). Indeed, the restricted permeability of the SGC host-rocks and relatively low temperatures (550–625 °C) estimated for the P–M intrusion have certainly concurred to inhibit major isotopic exchange reactions among minerals and between minerals and magmatic fluids, during contact metamorphism.

Moreover, the size and geometry of the outcropping P–M pluton suggest that magmatic fluid flow might have been very limited in its aureole, as in the case of the metapelitic-hosted Ballachulish igneous complex, in Scotland (Hoernes et al. 1991), where most of the magmatic water left the pluton through its roof, so that the aureole rocks retained their original heterogeneous sedimentary isotopic composition and show no systematic variation with distance to the intrusion.

Although the $\delta^{18}O$ signatures of the spotted-schists and hornfelses of the P–M contact-zone seem to be inherited from the regional host-rocks, and to depend on their variability, rather than on the thermal effects of the granitic intrusion, therefore preventing any distinction between the host

Table 5 Representative EMP data and structural formulae for biotite from regional SGC metasediments and from the spotted-schists and hornfelses of the Penamacor–Monsanto contact zone

	Regional pelitic rocks						Spotted-schists						Hornfelses					
	Biotites (4 an.)				Chl-Biot (2 an.)		Biotites (11 an.)				Chl-Biot (19 an.)		Biotites (30 an.)				Chl- Biot (2 an.)	
	An.1	An. 2	Average	Std. Dev.			An.1	An. 2	Average	Std. Dev.			An.1	An. 2	Average	Std. Dev.		
SiO_2	35.14	36.71	36.40	1.28	37.84	35.35	35.90	35.47	35.10	0.87	32.18	31.76	35.42	35.72	35.47	1.02	33.71	35.65
TiO_2	1.72	1.76	1.76	0.05	0.09	0.69	3.53	1.91	2.31	0.49	2.24	1.48	2.67	2.07	2.16	0.55	0.50	1.04
Al_2O_3	17.39	20.21	19.35	1.34	22.19	18.98	20.32	20.33	20.19	0.26	18.79	20.47	18.29	21.23	19.86	1.04	21.75	21.22
FeO	21.82	17.78	19.00	1.89	18.46	18.76	21.83	19.96	21.21	1.33	25.72	22.94	22.36	19.74	20.92	0.95	19.69	18.06
MnO	0.00	0.08	0.09	0.08	0.00	0.13	0.12	0.07	0.10	0.06	0.13	0.16	0.16	0.06	0.13	0.09	0.19	0.13
MgO	8.30	8.81	8.41	0.28	6.60	7.21	6.31	9.11	7.91	0.71	9.12	11.60	6.85	8.86	7.72	0.61	9.63	9.00
ZnO	0.00	0.00	0.10	0.17	0.26	0.00	0.00	0.00	0.04	0.07	0.00	0.00	0.17	0.04	0.07	0.09	0.12	0.00
BaO	0.00	0.13	0.08	0.06	0.11	0.06	0.08	0.11	0.09	0.07	0.20	0.03	0.23	0.00	0.16	0.07	0.06	0.06
CaO	0.23	0.00	0.06	0.12	0.50	0.61	0.00	0.03	0.04	0.04	0.03	0.08	0.00	0.00	0.02	0.05	0.19	0.43
Na_2O	0.13	0.03	0.07	0.04	0.07	0.06	0.04	0.12	0.10	0.05	0.08	0.05	0.14	0.11	0.13	0.05	0.09	0.07
K_2O	5.16	5.55	5.74	0.57	1.46	2.40	8.74	7.09	7.62	0.88	4.84	2.20	7.77	8.46	7.86	0.91	0.77	2.18
Rb_2O	0.00	0.05	0.06	0.05	0.04	0.07	0.04	0.00	0.03	0.02	0.05	0.01	0.03	0.03	0.09	0.11	0.00	0.04
F	0.28	0.19	0.20	0.12	0.00	0.21	0.13	0.11	0.12	0.11	–	–	0.04	–	0.69	0.95	–	–
Cl			0.00	0.00	0.04	–	0.00	0.00	0.01	0.01	0.00	0.00		–	0.01	0.00	0.02	0.02
Total	90.58	91.30	91.43	1.15	87.93	84.63	97.08	94.31	94.90	1.53	93.45	90.80	94.11	96.49	95.06	1.52	86.72	87.91
Cations per formula unit, on a basis of 11 oxygen atoms																		
Si	2.803	2.814	2.818	0.042			2.697	2.695	2.680	0.041			2.753	2.666	2.715	0.072		
Al^{IV}	1.197	1.186	1.182	0.042			1.303	1.305	1.320	0.041			1.247	1.334	1.285	0.072		
Al^{VI}	0.438	0.640	0.583	0.097			0.495	0.515	0.497	0.037			0.428	0.533	0.506	0.061		
Ti	0.103	0.101	0.102	0.002			0.199	0.109	0.133	0.027			0.156	0.116	0.124	0.031		
Fe	1.456	1.140	1.233	0.150			1.371	1.268	1.355	0.097			1.453	1.232	1.339	0.070		
Mn	0.000	0.005	0.006	0.005			0.007	0.004	0.007	0.004			0.010	0.004	0.008	0.006		
Mg	0.987	1.006	0.970	0.031			0.706	1.031	0.900	0.083			0.793	0.985	0.881	0.069		
Zn	0.000	0.000	0.005	0.010			0.000	0.000	0.002	0.004			0.009	0.002	0.004	0.005		
Ba	0.000	0.004	0.002	0.002			0.002	0.003	0.003	0.002			0.007	0.000	0.005	0.002		
Ca	0.020	0.000	0.005	0.010			0.000	0.003	0.003	0.003			0.000	0.000	0.001	0.004		
Na	0.020	0.005	0.011	0.007			0.005	0.017	0.015	0.008			0.021	0.016	0.019	0.007		
K	0.525	0.543	0.567	0.045			0.837	0.687	0.741	0.078			0.770	0.805	0.767	0.088		
Rb	0.000	0.002	0.003	0.002			0.002	0.000	0.001	0.001			0.001	0.002	0.004	0.006		
Total	7.549	7.447	7.488	0.045			7.627	7.638	7.657	0.051			7.650	7.696	7.660	0.064		
Mg/(Mg + Fe)	0.40	0.47	0.44	0.03			0.34	0.45	0.40	0.03			0.35	0.44	0.40	0.02		

The biotite and transitional chlorite–biotite analyses presented cover the Mg/(Mg + Fe) range obtained for each rock type

Table 6 Representative EMP data and structural formulae of cordierite from the spotted-schists and hornfelses of the Penamacor–Monsanto contact zone

	Cordierite in spotted-schists (6 an.)				Cordierite in hornfelses (10 an.)			
	An. 1	An. 2	Average	Std. Dev.	An. 1	An. 2	Average	Std. Dev.
SiO_2	48.08	48.28	48.66	0.47	48.19	48.48	48.48	0.46
TiO_2	0.02	0.03	0.01	0.01	0.00	0.06	0.02	0.03
Al_2O_3	33.36	32.70	33.26	0.30	32.80	33.47	32.81	0.44
FeO	11.19	10.43	10.51	0.85	10.42	9.23	9.84	0.53
MnO	0.20	0.16	0.18	0.09	0.10	0.27	0.23	0.10
MgO	5.82	6.50	6.50	0.52	6.66	7.10	6.91	0.22
ZnO	0.11	–	0.04	0.05	0.06	0.00	0.05	0.10
BaO	0.06	0.06	0.06	0.01	0.02	0.08	0.08	0.04
CaO	0.02	0.01	0.01	0.01	–	0.06	0.01	0.02
Na_2O	0.55	–	0.23	0.26	0.21	0.46	0.31	0.08
K_2O	0.00	0.00	0.00	0.00	0.00	0.00	0.00	0.00
Total	99.45	98.18	99.46	0.94	98.54	99.23	98.77	0.68
Cations per formula unit, calculated on a basis of 18 oxygen atoms								
Si	4.973	5.023	5.004	0.022	5.004	4.981	5.020	0.045
Al^{IV}	1.027	0.977	0.996	0.022	0.996	1.019	0.980	0.045
Al^{VI}	3.040	3.033	3.035	0.015	3.018	3.015	3.015	0.008
Ti	0.002	0.002	0.001	0.001	0.000	0.000	0.002	0.002
Fe	0.968	0.908	0.904	0.072	0.905	0.772	0.826	0.044
Mn	0.017	0.014	0.016	0.008	0.009	0.031	0.021	0.008
Mg	0.897	1.008	0.996	0.079	1.031	1.139	1.074	0.035
Zn	0.008	0.000	0.003	0.004	0.004	0.003	0.001	0.001
Ba	0.003	0.003	0.002	0.001	0.001	0.003	0.004	0.001
Ca	0.002	0.001	0.001	0.001	0.000	0.000	0.002	0.002
Na	0.109	0.000	0.046	0.051	0.042	0.076	0.072	0.013
K	0.000	0.000	0.000	0.000	0.000	0.000	0.000	0.000
Total	11.046	10.969	11.003	0.038	11.010	11.040	11.017	0.026
Mg/(Mg + Fe)	0.48	0.53	0.52	0.04	0.53	0.58	0.57	0.02

The two cordierite analyses presented for each rock type cover the Mg/(Mg + Fe) range obtained

SGC rocks and contact-zone rocks, or even between hornfelses and spotted-schists, it cannot be completely excluded that restricted, very localized temperature-related isotope exchange may have occurred, probably in the presence of magmatic fluid exiting from the cooling intrusion. A few low $\delta^{18}O$ values (~ 13‰) recorded on contact rocks nearest to the pluton may indeed represent isotopic departures from the original country-rock values and correspond to thermally-induced isotopic reequilibration.

5.3 Thermal anisotropy along the contact aureole

Bulk-rock isotopic composition (e.g. Nabelek 1991) and geothermometers based on Ti content and Mg/(Mg + Fe) ratio in biotite (e.g. Henry and Guidotti 2002; Henry et al. 2005) have been proposed to ascertain thermal gradient variations, and consequent heat flux variations, associated with the emplacement of granites at different temperatures. In the P–M aureole, however, although there seems to be some correlation between Ti contents in biotite and whole-rock $\delta^{18}O$ (Fig. 12), no systematic relationship was found between any of these two parameters and the temperatures estimated for granite intrusion along the contact aureole.

The only likely, though unconfirmed, evidence of thermal anisotropy along the granite–host contact is the concentric textural zonation observed in the ghost cordierite porphyroblasts of a few spotted-schists (samples P-16 and P-18; Ribeiro da Costa et al. 2013) from the NW zone of the metamorphic aureole, close to the lower-T marginal granites. Micro-inclusions within porphyroblasts of spotted-schists from zones of the contact aureole where granites have intruded at higher temperatures are texturally homogeneous in grain size and mineralogy. Porphyroblast texture might, therefore, be a good indicator of thermal anisotropy related to the emplacement of different marginal granites. Indeed, at the low- to intermediate-grade conditions which characterize the P–M contact aureole, the rate of volume diffusion is minor and recrystallization is needed for mineral grains to

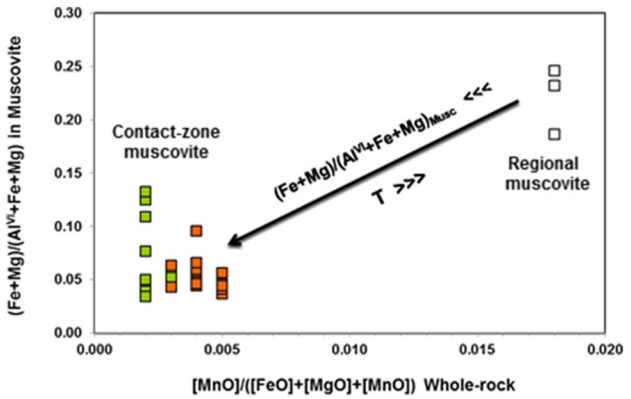

Fig. 8 Temperature-related correlation between the (Mg + Fe)/(Al^{VI} + Mg + Fe) ratio in muscovites and bulk-rock [MnO]/([MgO] + [FeO] + [MnO]) ratios, showing a marked decrease in the proportion of (Mg + Fe) in muscovites and of bulk-rock MnO from regional metasediments to spotted-schists and hornfelses, i.e., with increasing metamorphic grade. Symbols as in Fig. 5

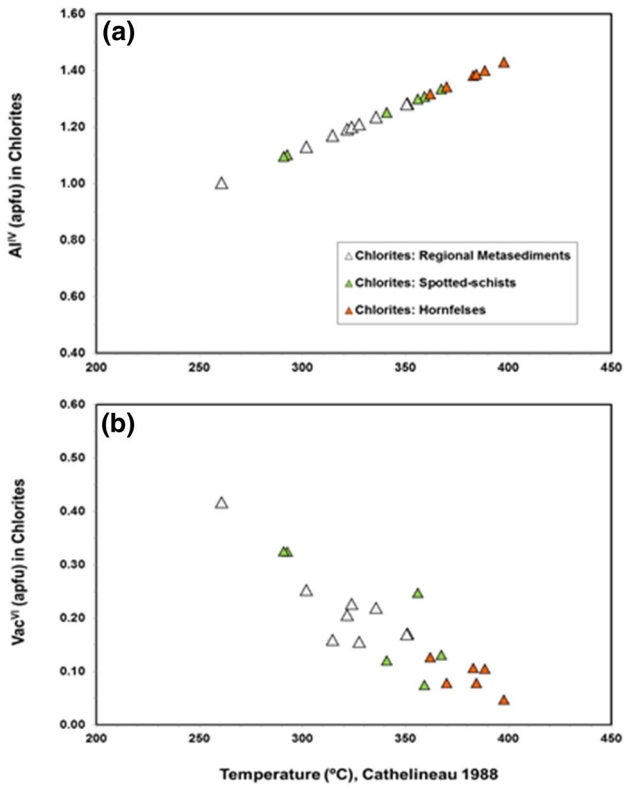

Fig. 9 **a** Temperatures obtained for the Penamacor–Monsanto contact-zone and host metasediments, using the Cathelineau (1988) termomether, based on the Al^{IV} proportion in chlorite; **b** in agreement with de Caritat et al. (1993), vacancies in the octahedral position of chlorites decrease with increasing temperatures (calculated by the Cathelineau 1988 method)

achieve equilibrium (Dowty 1980; Worley et al. 1997), so they are often complexly zoned, thus providing some critical information for thermodynamic interpretation of mineral assemblages (Vernon and Clarke 2008).

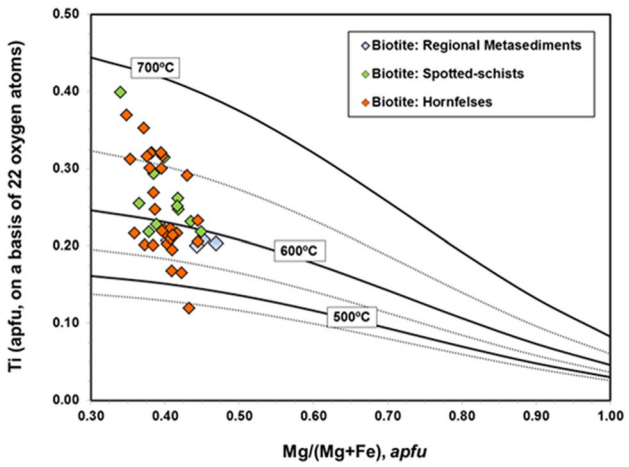

Fig. 10 Ti vs. Mg/(Mg + Fe) distribution in biotites from Penamacor–Monsanto contact rocks and host rocks. Isotherms determined experimentally by Henry et al. (2005) suggest some contact-zone biotites may have formed at temperatures as high as ~ 700 °C, in clear contradiction with other evidence

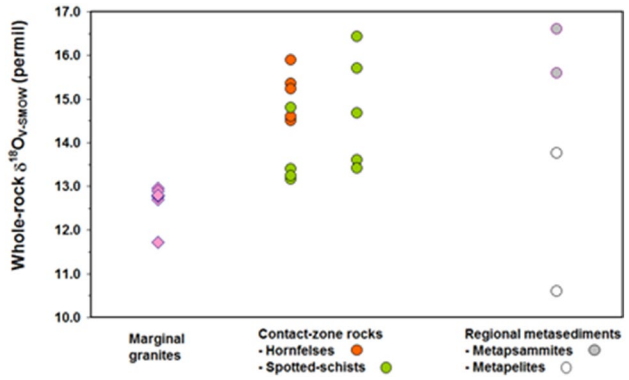

Fig. 11 Plot of $\delta^{18}O$ data for the P–M marginal granitic rocks (data from Ribeiro da Costa et al. 2014), contact-zone rocks (hornfels and spotted-schists) and close regional SGC metasediments

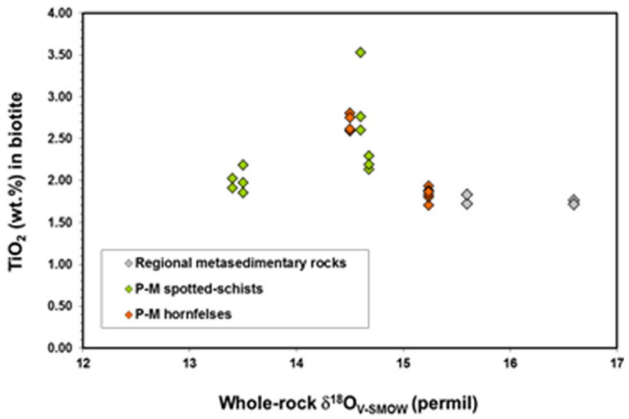

Fig. 12 Correlation between TiO_2 contents in biotite and the whole-rock $\delta^{18}O$ values for the respective regional metasediments and contact-zone rocks

6 Conclusions

Superimposed on the regional chlorite-zone metamorphism, contact metamorphism associated to the emplacement of the P–M granitic pluton has little cartographic representation: the metamorphic aureole is narrow and irregular, made up of fine-grained spotted-schists and rarer hornfelses. The textures and mineral compositions grade towards those typical of regional metamorphism, in the outer zones of the aureole. As described in many other metamorphic aureoles set in low- to intermediate-grade metapelitic sediments, the effects of contact metamorphism caused by the P–M intrusion are, therefore, not always easy to distinguish from the regional background, especially due to the late weathering affecting the pluton and host metasediments.

In spite of these constraints, some important conclusions have been achieved in this study.

(i) Mineral parageneses (Ms + Bt + Chl + Crd ± Qz ± Pl, in spotted-schists; Bt + Chl + Qz + Ms + Pl ± Crd, in hornfelses) and the composition of coexisting mineral phases indicate that most contact rocks attained the *biotite zone* (or even the *cordierite zone*, in some cases), i.e., upper greenschist—lower amphibolite grade. This is consistent with the temperatures estimated for the emplacement of the P–M granites (Ribeiro da Costa et al. 2014).

(ii) A few significant textural and mineralogical features distinguish these contact-zone rocks from the host SGC metasediments, namely the ubiquitous presence of relic or ghost cordierites in the spotted-schists and some hornfelses, some evidence of recrystallization in hornfelses, and the Al-richer composition of contact-rock muscovite.

(iii) However, the spatial variation in textures and mineral assemblages of the contact rocks surrounding the P–M intrusion, their bulk-rock geochemistry and oxygen isotope signatures seem to reflect the metapelitic or metapsammitic character of regional host-rocks, rather than thermal variations within the aureole. The features of the contact aureole seem indeed to be more strongly controlled by the textural, mineralogical, geochemical and isotopic heterogeneity of the SGC metasediments than by kinetic factors, though the latter may occasionally be significant in the rocks closest to the intrusion margins, which have been subjected to higher heating rates than those typically associated with regional metamorphism.

(iv) The fact that geochemical and isotopic *nuances* between the hornfelses and spotted-schists of the P–M contact aureole are mainly related to the heterogeneities of regional metasediments, rather than to thermal effects due to the emplacement of the P–M intrusion, imply that (a) the temperatures of emplacement of the P-M marginal granites (estimated at 550–625 °C) were not high enough to produce significant chemical or isotopic diffusion gradients, (b) interaction of magmatic-derived fluids and host-rock may have been insufficient to promote such effects, and/or (c) host SGC rocks are too unreactive to effectively record more distinct evidence of thermal effects due to granite emplacement.

(v) The presence or absence of textural zonation in cordierite porphyroblasts seems to be the only likely indicator of thermal anisotropy along the contact aureole. The absence of more definite and widespread indicators of thermal anisotropy implies that heat flux variations along the pluton border were necessarily limited, in good agreement with the narrow range of temperatures estimated for the emplacement of the P–M marginal granites.

(vi) The narrow metamorphic aureole associated with the P–M pluton and relatively low crystallization temperatures obtained for its granitic rocks, and the restricted isotopic and mineralogical effects observed on the host SGC rocks, suggest that the P–M massif may correspond to the uppermost part of a larger granitic intrusion.

Acknowledgements We are most grateful to Mr. Alberto Verde (GeoFCUL) who prepared the polished thin-sections used in this study. Dr. Narciso Ferreira (LNEG, S. Mamede de Infesta) generously provided very useful field information concerning contact-zone outcrops around the P–M pluton. Mr Felix García García (Univ. Salamanca) helped with stable isotope determinations.

Funding Funding was provided by FCT—Fundação para a Ciência e Tecnologia, through project METMOB (PTDC/CTE-GIX/116204/2009)—"*Elementar and isotopic mobility and diffusion in metamorphic minerals from granite contact aureoles*".

References

Ábalos, B., Carreras, J., Druguet, E., Viruete, J. E., Pugnaire, M. T. G., Alvarez, S. L., et al. (2002). Variscan and Pre-Variscan Tectonics. In W. Gibbons & M. T. Moreno (Eds.), *The geology of Spain*. London: Geological Society.

Acciaioli, M. H., Santos, J. F., & Munhá, J. M. (2005). Ar-Ar dates for two different stages of the Variscan D3 recorded in metapelites of Serra da Freita (North - Central Portugal). *Geophysical Research Abstracts, 7,* 10076.

Antunes, I. M. H. R., Neiva, A. M. R., Silva, M. M. V. G., & Corfu, F. (2009). The genesis of I- and S-type granitoid rocks of the Early Ordovician Oledo pluton, Central Iberian Zone (central Portugal). *Lithos, 111,* 168–185.

Azevedo, M.R., Valle Aguado, B., Nolan, J., Martins M., Medina J. (2005). Origin and emplacement of syn-orogenic Varsican granitoids in Iberia: the Beiras massif. In: Carosi R., Dias R., Lacopini D., Rosenbaum G. (Eds.), *The southern Variscan belt,*

Journal of the Virtual Explorer, Electronic Edition, vol. **19**, Paper 7.

Bea, F., Sanchez González de Herrero, J.G., Serrano Pinto, M. (1987). Una compilación geoquímica elementos mayores para los granitoides del macizo Hespérico. In: Bea et al. (Eds.), *Geología de los granitoides y rocas asociadas del macizo Hespérico*. Ed. Rueda, pp. 87-193.

Beetsma, J.J. (1995). The Late Proterozoic/Paleozoic and Hercynian cristal evolution of the Iberian Massif, N Portugal. PhD Thesis, Vrije University, Amsterdam.

Blamart, D. (1991). Les concentrations tungstifères et stannifères: caractérisation isotopique (H–O) des fluides minéralisateurs, sur l'exemple du gisement Sn–W de Walmes (Maroc central). Détermination de quelques fractionnements isotopiques (H–O) entre minéraux et eaux. Thèse de doctorat, Institut National Polytechnique de Lorraine.

Borthwick, J., & Harmon, R. S. (1982). A note regarding CIF3 as an alternative to Br F5 for oxygen isotope analysis. *Geochimica et Cosmochimica Acta, 46,* 1665–1668.

Castro, A., Corretgé, L. G., Enrique, P., Martínez, F. J., Pascual, E., Lago, M., et al. (2002). Paleozoic Magmatism. In W. Gibbons & T. Moreno (Eds.), *The geology of Spain* (pp. 117–153). London: Geol. Soc. London.

Cathelineau, M. (1988). Cation site occupancy in chlorites and illites as a function of temperatura. *Clay Minerals, 23,* 471–485.

Clayton, R. N., & Mayeda, T. K. (1963). The use of bromine pentafluoride in the extraction of oxygen from oxides and silicates for isotopic analysis. *Geochimica et Cosmochimica Acta, 27,* 43–52.

Conde, L.E.N., Rachinhas, P.C.R.S., Rabaça, T.J.L. (2000). Aspectos metalogenéticos da região de Castelo-Branco: parâmetros controladores das mineralizações e abordagem dos impactes ambientais associados. Dept. Ciências da Terra, Faculdade de Ciências e Tecnologia, Universidade de Coimbra. Relatório do Projecto Praxis XXI - 2/2.1/CTA/81/94. Cap. IV: Geologia Regional, 13–17.

De Caritat, P., Hutcheon, I., & Walshe, J. L. (1993). Chlorite geothermometry: a review. *Clays and Clay Minerals, 41*(2), 219–239.

Dias, G., Ferreira, N., Leterrier, J., & Pereira, E. (1998). Petrogénese de associações ácidas-básicas no contexto do plutonismo tardi-hercínico: o exemplo do maciço granítico de Celorico de Basto (Norte de Portugal). *Comunicações do IGM, 84*(1), B51–B54.

Dowty, E. (1980). Crystal-chemical factors affecting the mobility of ions in minerals. *American Mineralogist, 65,* 174–182.

Ernst, W. G. (1963). Significance of phengitic micas from low-grade schists. *American Mineralogist, 48,* 1357–1373.

Evans, B. W., & Guidotti, C. V. (1966). The sillimanite-potash feldspar isograd in Western Maine, USA. *Contributions to Mineralogy and Petrology, 12,* 25–62.

Ferreira, N., Iglésias, M., Noronha, F., Pereira, E., Ribeiro, A., & Ribeiro, M. L. (1987). Granitóides da zona Centro-Ibérica e seu enquadramento geodinâmico. In F. Bea, A. Carmina, J. C. Gonzalo, M. L. Plaza, & J. M. L. Rodrigues (Eds.), *Geologia de los granitoides y rocas asociadas del Macizo Hespérico* (pp. 37–53). Madrid: Libro Homenage a L.C.G. Figueirola. Editorial Rueda.

Ferreira Pinto, A.F. & Matos, C.A.R. (2000). Aspectos metalogenéticos da região de Castelo-Branco: parâmetros controladores das mineralizações e abordagem dos impactos ambientais associados. Dept. Ciências da Terra, Faculdade de Ciências e Tecnologia, Universidade de Coimbra. *Relatório do Projecto Praxis XXI - 2/2.1/CTA/81/94*. Cap. V: Alguns Aspectos da Petrologia, 18-50.

Gama Pereira, L. C. (1976). Notícia sobre o "Complexo Xisto-Grauváquico" entre Capinha e Penamacor. *Memórias e Notícias, 82,* 61–66. **(Publ. Mus. Lab. Mineral. Geol. Univ. Coimbra)**.

Gutiérrz-Alonso, G., Fernández-Suárez, J., Jeffries, T. R., Johnston, S. T., Pastor-Galán, D., Murphy, J. B., et al. (2011). Diachronous post-orogenic magmatism within a developing orocline in Iberia, European Variscides. *Tectonics, 30,* 1–17.

Henry, D. J. & Dutrow, B. L. (1996). Metamorphic tourmaline and its petrologic applications. In E. S. Grew & L. M. Anovitz (Eds.), *Boron: Mineralogy, petrology and geochemistry. Mineral. Soc. Am. Rev. Mineral*, chp 10 (vol. 33).

Henry, D. J., & Guidotti, C. V. (2002). Titanium in biotite from metapelitic rocks: Temperature effects, crystal-chemical controls, and petrologic applications. *American Mineralogist, 87,* 375–382.

Henry, D. J., Guidotti, C. V., & Thomson, J. A. (2005). The Ti-saturation surface for low-to-medium pressure metapelitic biotite: implications for geothermometry and Ti-substitution mechanisms. *American Mineralogist, 90,* 316–328.

Hoernes, S., Macleod-Kinsell, S., Harmon, R. S., Pattison, D. R. M., & Strong, D. F. (1991). Stable isotope geochemistry on the intrusive complex and its metamorphic aureole. In G. Voll, J. Topel, D. R. M. Pattison, & F. Seifert (Eds.), *Equilibrium and kinetics in contact metamorphism: the Ballachulish Igneous Complex and its thermal aureole*. Heidelberg: Springer.

Ishikawa, Y., Sawaguchi, T., Iwaya, S., & Honuchi, M. (1976). Delineation of prospecting targets for kuroko deposits based on modes of volcanism of underlying dacite and alteration halos. *Mining Geology, 26,* 105–117. **(in Japanese with English abstract)**.

Johnson, S. E. (1992). Sequential porphyroblast growth during progressive deformation and low-P high-T (LPHT) metamorphism, Cooma Complex, Australia: the use of microstructural analysis in better understanding deformation and metamorphic histories. *Tectonophysics, 214,* 311–339.

London, D. (1999). Stability of tourmaline in peraluminous granite systems: the boron cycle from anatexis to hydrothermal aureoles. *European Journal of Mineralogy, 11,* 253–262.

Miller, T., Baumgartner, L. P., Foster, C. T., & Venneman, T. W. (2004). Metastable prograde mineral reactions in contact aureoles. *Geology, 32,* 821–824.

Miyashiro, A. (1978). *Metamorphism and metamorphic belts* (p. 492). London: George, Allen & Unwin.

Miyashiro, A. (1994). *Metamorphic Petrology* (p. 404). London: UCL Press.

Nabelek, P. L. (1991). Stable isotope monitors. In D. M. Kerrick (Ed.), *Contact metamorphism. Mineral. Soc. Am. Rev. Mineral*, chp 9 (vol. 26, pp. 395–435). USA: Mineralogical Society of America.

Neiva, A. M. R., & Campos, T. F. C. (1992). Genesis of the zoned granitic pluton of Penamacor–Monsanto, Central Portugal. *Memórias e Notícias. Memórias e Notícias, 114,* 51–68. **(Publ. Mus. Lab. Mineral. Geol. Univ. Coimbra)**.

Neiva, A. M. R., & Campos, T. F. C. (1993). The zoned granitic pluton of Penamacor–Monsanto, Central Portugal: hydrothermal alteration. *Memórias e Notícias, 116,* 21–47. **(Publ. Mus. Lab. Mineral. Geol. Univ. Coimbra)**.

Neiva, A. M. R., Williams, I. S., Ramos, J. M., Gomes, M. E. P., Silva, M. M. V. G., & Antunes, I. M. H. R. (2009). Geochemical and isotopic constraints on the petrogenesis of Early Ordovician granodiorite and Variscan two-mica granites from the Gouveia area, central Portugal. *Lithos, 111,* 186–202.

Oen, Y.S. (1970). Granite intrusion, folding and metamorphism in central northern Portugal. *Bol. Geol. Minero*, tomo **LXXXI**, fasc. II-III, 271–298.

Oliveira, J. T., Pereira, E., Ramalho, M., Antunes, M. T., & Monteiro, J. H. (1992). *Carta Geológica de Portugal na escala 1/500 000* (5ª ed.). Lisboa: Serviços Geológicos de Portugal.

Pattison, D. R. M. (1987). Variations in Mg/(Mg + Fe), F, and (Fe, Mg) Si = 2Al in pelitic mineralsin the Ballachulish thermal aureole, Scotland. *American Mineralogist, 72,* 255–272.

Pattison, D. R. M. & Tracy, R. J. (1991). Phase equilibria and thermobarometry of metapelites. In D. M. Kerrick (Ed.), *Contact*

metamorphism. Mineral. Soc. Am. Rev. Mineral., chp 4 (vol. 26, pp. 105–206). USA: Mineralogical Society of America.

Pesquera, A., Torres-Ruiz, J., García-Casco, A., & Gil-Crespo, P. P. (2013). Evaluating the controls on tourmaline formation in granitic systems: a case study on peraluminous granites from the Central Iberian Zone (CIZ), Western Spain. *Journal of Petrology, 54*(3), 609–634.

Ramírez, J. A., & Grundvig, S. (2000). Causes of geochemical diversity in peraluminous granitic plutons: the Jalama pluton, Central-Iberian Zone (Spain and Portugal). *Lithos, 50,* 171–190.

Reavy, R. J. (1989). Structural controls on metamorphism and syntectonic magmatism: the Portuguese Hercynian collision belt. *Journal of the Geological Society London, 146,* 649–657.

Ribeiro da Costa, I., Antunes, I.M.H.R., Farinha Ramos, J.M., Recio, C., Barriga, F.J.A.S., Mourão, C., Guimarães, F., Ferreira, N. (2013). Aspectos petrográficos do metamorfismo de contacto associado ao plutão granítico de Penamacor-Monsanto. *Comun. Geológicas*, *100*(1), 89–98. http://www.lneg.pt/iedt/unidades/16/paginas/26/30/141

Ribeiro da Costa, I., Mourão, C., Recio, C., Guimarães, F., Antunes, I. M. H. R., Farinha Ramos, J. M., et al. (2014). Tourmaline occurrences within the Penamacor–Monsanto granitic pluton and host-rocks (Central Portugal): genetic implications of crystal-chemical and isotopic features. *Contributions to Mineralogy and Petrology, 167*(4), 993–1115.

Ribeiro, A., Quesada, C., & Dallmeyer, R. D. (1990). Geodynamic evolution of the Iberian Massif. In R. D. Dallmeyer & G. Martinez (Eds.), *Pre-Mesozoic geology of Iberia* (pp. 399–409). Berlin: Springer.

Savin, S. M., & Epstein, S. (1970). Oxygen and hydrogen isotope geochemistry of clay minerals. *Geochimica et Cosmochimica Acta, 34,* 25–42.

Sharp, Z. (1990). A laser-based microanalytical method for the in situ determination of oxygen isotope ratios of silicates and oxides. *Geochimica et Cosmochimica Acta, 54,* 1353–1357.

Sheppard, S.M.F. (1986). Characterization and isotopic variations in natural waters. In: Valley, J.W., Taylor, H.P. and O'Neil, J.R. (eds.), Stable Isotopes in High Temperature Geological Processes. *Reviews in Mineralogy, 16*, 165-183.

Shieh, Y. N. & Taylor, H. P. Jr. (1969). Oxygen and hydrogen isotope studies of contact metamorphism in the Santa Rosa Range, Nevada and other areas. *Contributions to Mineralogy and Petrology, 20,* 306–356.

Sousa, M. B. (1985). Perspectiva sobre os conhecimentos actuais do Complexo Xisto- Grauváquico de Portugal. *Memórias e Noticias, 100,* 1–16. **(Publ. Mus. Lab. Mineral. Geol. Univ. Coimbra)**.

Taylor, H. P. (1974). The application of oxygen and hydrogen isotope studies to problems of hydrothermal alteration and ore deposition. *Economic Geology, 69*(6), 843–883.

Thompson, A. B. (1976). Mineral reactions in pelitic rocks, I and II. *American Journal of Science, 276*(401–424), 425–454.

Ugidos, J. M. (1990). Granites as a paradigm of genetic processes of granitic rocks: I-types vs S-types. In R. D. Dallmeyer & E. Martinez (Eds.), *Pre-Mesozoic geology of Iberia* (pp. 189–206). Berlin,: Springer-Verlag.

Ugidos, J. M., Sánchez-Santos, J. M., Barba, P., & Valladares, M. I. (2010). Upper Neoproterozoic series in the Central Iberian, Cantabrian and West Asturian LeoneseZones (Spain): geochemical data and statistical results as evidence for a shared homogenised source area. *Precambrian Research, 178,* 51–58.

Valladares, I., Ugidos, J. M., & Recio, C. (1993). Criterios geoquímicos de correlación y posible área fuente de las pelitas del Precámbrico superior – Cámbrico inferior de la Zona Centro-Ibérica (Macizo Ibérico, España). *Revista de la Sociedad Geológica de España, 6*(1–2), 37–45.

Vernon, R. H., & Clarke, G. L. (2008). *Principles of metamorphic petrology* (p. 446). Cambridge: Cambridge University Press.

Villaseca, C., Merino, E., Oyarzun, R., Orejana, D., Pérez-Soba, C., & Chicharro, E. (2014). Contrasting chemical and isotopic signatures from Neoproterozoic metasedimentary rocks in the Central Iberian Zone (Spain) of pre-Variscan Europe: implications for terrane analysis and Early Ordovician magmatic belts. *Precambrian Research, 178,* 131–145.

Vindel, E., Chicharro, E., Villaseca, C., López-García, J. A., & Sánchez, V. (2014). Hydrothermal phosphate vein-type ores from the southern Central Iberian Zone, Spain: evidences for their relationship to granites and Neoproterozoic metasedimentary rocks. *Ore Geology Reviews, 62,* 143–155. https://doi.org/10.1016/j.oregeorev.2014.03.011.

Voll, G., Töpel, J., Pattison, D. R. M., & Seifert, F. (Eds.). (1991). *Equilibrium and kinetics in contact metamorphism: the Ballachulish igneous complex and its aureole*. Berlin: Springer-Verlag.

White, A. J. R., & Chappell, B. W. (1988). Some supracrustal (S-type) granites of the Lachlan Fold Belt. *The Royal Society of Edinburgh Earth Science, 79,* 169–181.

Whitney, D. L., & Evans, B. W. (2010). Abbreviations for names of rock-forming minerals. *American Mineralogist, 95,* 185–187.

Worley, B., Powell, R., & Wilson, C. J. L. (1997). Crenulation cleavage formation: evolving diffusion, deformation and equilibrium mechanisms with increasing metamorphic grade. *Journal of Structural Geology, 19*(8), 121–1135.

Zheng, Y. F. (1993). Calculation of oxygen isotope fractionation in hydroxyl-bearing silicates. *Earth and Planetary Science Letters, 120,* 247–263.

Affiliations

Isabel Ribeiro da Costa[1] · Isabel Margarida H. R. Antunes[2] · Cyntia Mourão[1,3] · Clemente Recio[4] · Fernanda Guimarães[5] · João Farinha Ramos[3] · Fernando J. A. S. Barriga[1,3]

✉ Isabel Ribeiro da Costa
imscosta@fc.ul.pt

[1] Departamento de Geologia, Faculdade de Ciências, Universidade de Lisboa, Bloco C6-4º Piso, Campo Grande, 1749-016 Lisbon, Portugal

[2] ICT Research Centre/Universidade do Minho, Braga, Portugal

[3] IDL-Instituto D. Luiz (Laboratório Associado), Lisbon, Portugal

[4] Departamento de Geología, Universidad de Salamanca, Salamanca, Spain

[5] Laboratório Nacional de Energia e Geologia (LNEG), S. Mamede de Infesta, Portugal